ADVANCED FUNCTIONAL MATERIALS
www.afm-journal.de

Covalent Organic Frameworks for Batteries

Dongyang Zhu, Guiyin Xu, Morgan Barnes, Yilin Li, Chia-Ping Tseng, Zhuqing Zhang, Jun-Jie Zhang, Yifan Zhu, Safiya Khalil, Muhammad M. Rahman,* Rafael Verduzco,* and Pulickel M. Ajayan**

Covalent organic frameworks (COFs) have emerged as an exciting new class of porous materials constructed by organic building blocks via dynamic covalent bonds. They have been extensively explored as potentially superior candidates for electrode materials, electrolytes, and separators, due to their tunable chemistry, tailorable structures, and well-defined pores. These features enable rational design of targeted functionalities, facilitate the penetration of electrolytes, and enhance ion transport. This review provides an in-depth summary of the recent progress in the development of COFs for diverse battery applications, including lithium-ion, lithium–sulfur, sodium-ion, potassium-ion, lithium–CO_2, zinc-ion, zinc–air batteries, etc. This comprehensive synopsis pays particular attention to the structure and chemistry of COFs and novel strategies that have been implemented to improve battery performance. Additionally, current challenges, possible solutions, and potential future research directions on COFs for batteries are discussed, laying the groundwork for future advances for this exciting class of material.

1. Introduction

Due to steady growth in worldwide energy usage and a shift toward renewable sources of energy, there is a need for innovative energy storage solutions such as batteries. Batteries can help increase the utilization of renewable energy and potentially reduce the demand for power supply during peak usage. For example, batteries enable a transition to electric vehicles[1–3] and offer solutions for storing sustainable sources of energy, including solar and wind.[1,2,4,5] There is a growing interest in the development of various battery technologies (**Figure 1**a,b), and improvements in energy densities, cycling stabilities, and safety are needed to meet the demand for energy storage.

These improvements can be achieved through the development or discovery of new materials that can be used in battery electrodes, electrolytes, or separators. A variety of porous materials have been studied and developed for use in batteries, including covalent organic frameworks (COFs),[6] metal-organic frameworks (MOFs),[6] and porous organic polymers (POPs).[7] These materials are attractive for energy storage applications because they all share tunable chemistry and structures, and their porous architecture facilitates the penetration of electrolyte and ion transport. They can be designed with redox-active functionalities or other functionalities to increase charge storage capacity or improve ion mobility.[6–10] Among them, COFs are crystalline and porous materials built from modular organic building blocks.[11–13] Compared to MOFs, COFs have lower molecular weight and higher energy density since they are composed of light elements (C, H, N, O, B, etc.). COFs also display excellent stability in various solvents,[14] while the stability of MOFs is still a challenging problem.[15] Furthermore, the skeletons of COFs are composed of different organic linkers, while the skeletons of MOFs are constructed by metal ions and organic linkers, so it is easier to design more functionalities in COFs to realize the targeted properties. Compared to amorphous POPs with disordered structures, COFs have more ordered pore channels, facilitating ion transport. Crystalline structures of COFs also make it possible to predict their properties through theoretical simulations. Therefore, COFs have recently received growing interest (Figure 1c), including energy storage (Figure 1d). Publications on COFs and COF batteries have increased steadily in recent years (Figure 1c,d).

COFs have been extensively studied in the application of different batteries, including lithium-ion batteries (LIBs), lithium–sulfur batteries (Li-S), sodium-ion batteries (SIBs), potassium-ion batteries (PIBs), zinc-ion batteries (ZIBs), zinc–air batteries (Zn-air), lithium–CO_2 batteries (Li-CO_2) and lithium-silicon (Li-Si) batteries (**Figure 2**). The organic nature

Dr. D. Zhu, Dr. Y. Li, C.-P. Tseng, Z. Zhang, S. Khalil, Prof. R. Verduzco
Department of Chemical and Biomolecular Engineering
Rice University
Houston, TX 77005, USA
E-mail: rafaelv@rice.edu
Dr. G. Xu
Department of Nuclear Science and Engineering
Massachusetts Institute of Technology
Cambridge, MA 02139, USA
E-mail: xuguiyin@mit.edu
M. Barnes, Dr. J.-J. Zhang, Y. Zhu, Dr. M. M. Rahman, Prof. R. Verduzco, Prof. P. M. Ajayan
Department of Materials Science and NanoEngineering
Rice University
Houston, TX 77005, USA
E-mail: mr64@rice.edu; ajayan@rice.edu
The ORCID identification number(s) for the author(s) of this article can be found under https://doi.org/10.1002/adfm.202100505.

DOI: 10.1002/adfm.202100505

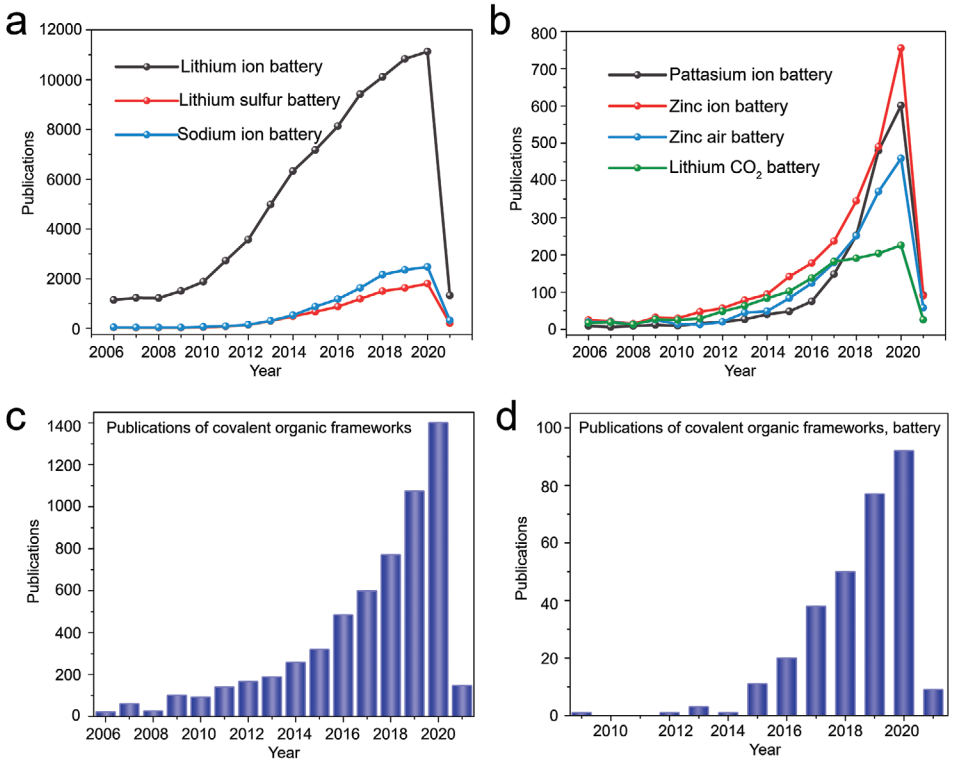

Figure 1. Publication numbers by topic over time. Data from Web of Science March 2021 by searching the topic, a) lithium-ion battery, lithium–sulfur battery, sodium-ion battery, potassium-ion battery, zinc ion battery, zinc–air battery and lithium–CO_2 battery, b) covalent organic frameworks, c) covalent organic frameworks, battery.

of COFs endows them with tunable chemistry and tailorable structures.[14] The redox-active sites can be predesigned into COF precursors with precise density and positions to alter the energy density of electrode materials.[16] Organic functionalities that promote metal ion mobility can also be precisely anchored in the structure of COFs, and thus overcome the sluggish ion transport drawbacks in batteries.[17,18] Additionally, functionalities that can chemically interact with sulfur can be embedded in COF backbones, increase sulfur loading, and reduce sulfur loss during the charge-discharge process.[19–21] 2D layered structures of COFs ensure the ordered straightforward 1D pore channels that facilitate the ion transport and reduce resistance compared to complicated interlaced pore channels.[18] 2D layered structures also provide possibilities to control the thickness of COFs and give access to few-layered nanosheets that are desired in battery applications.[8] By taking advantage of these features, researchers managed to tackle the challenges in battery applications and improve their electrochemical performance.

In this review, we focus on the applications of COFs and COF composites in different electrochemical batteries, mainly LIBs, Li-S batteries, and other novel and emerging batteries, as illustrated in Figure 2. We summarize the latest progress and pay particular attention to the new structures and chemistries of COFs and novel strategies implemented to improve their performance. Finally, we will discuss the challenges in COF battery areas, put forward possible strategies to address current problems, and propose future potential research directions.

2. Application of COFs in LIBs

LIBs are the most promising energy storage technology for transportation applications. While lead-acid batteries are cheaper, more mature, and more widely used in vehicles, they do not produce sufficient power to replace internal combustion engines.[22] LIBs are superior to lead-acid batteries in capacity, efficiency, lifespan, and power.[23,24] Conventional LIBs are composed of a graphite anode,[3,4,25] transition metal oxide cathode (e.g., $LiCoO_2$, $LiFePO_4$, and $LiMn_2O_4$),[23,26,27] electrolyte,[23,28–32] and membrane separator.[33–36] However, conventional LIBs cannot provide charge capacities greater than 200 mAh g^{-1} due primarily to the limited energy storage capacity of the cat hode.[3,23,25,27,37,38] Conventional LIBs also suffer from significant capacity fade over repeated use, necessitating frequent replacement.[25,27,37,38] Therefore, there is a need for new materials and approaches that can increase both the capacity and lifespan of LIBs.

Inorganic battery materials generally offer higher energy storage capacities than organics;[3,25–27] however, organic materials provide several advantages, including lower cost, more abundant feedstocks, and greater sustainability.[3,4,6,8–10,26] However, it remains challenging to achieve high capacity and long cycle stability for organic electrodes since they have relatively low conductivity and weak structural stability.[39–41] COFs provide several unique characteristics beneficial to electrode performance, including porous functional structures and excellent chemical and thermal stabilities.[6,8–10] This section will

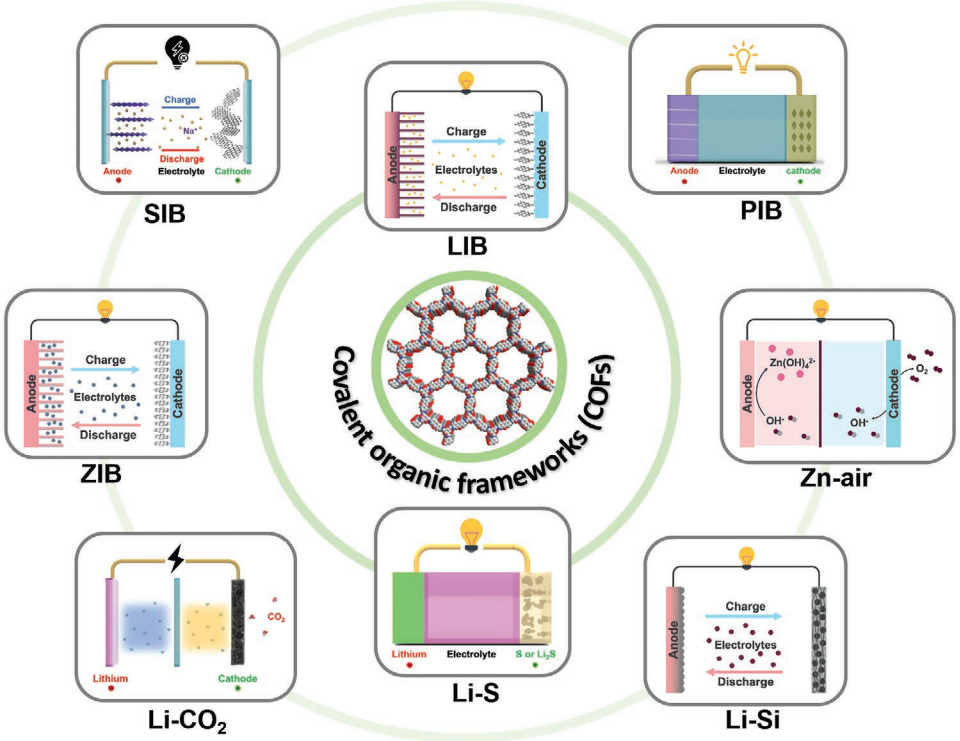

Figure 2. Schematics of COFs for different battery applications including lithium-ion batteries (LIB), lithium–sulfur batteries (Li-S), sodium-ion batteries (SIB), potassium-ion batteries (PIB), zinc-ion batteries (ZIB), and zinc–air batteries (Zn-air), lithium–CO_2 batteries (Li-CO_2) and lithium-silicon batteries (Li-Si).

comprehensively summarize current studies of COFs in LIBs, including their applications in the anode, cathode, electrolyte, and separator.

2.1. Anode

The anode is also known as the negative electrode, releases Li-ions to the electrolyte in the discharge process and receives Li-ions in the charging process.[3,4,25,38,42] Currently, the most popular anode materials are carbon-based materials (e.g., commercial graphite) and porous, core-shell structures.[3,4,25] Current experimental studies of COF anodes mainly focus on COFs with conjugated structures and a high density of redox-active sites,[43–48] hybrids of COFs with carbon materials (e.g., carbon nanotubes (CNT), graphene)[49] to enhance the electron conductivity and cycle stability, and exfoliated COF nanosheets[50–53] to shorten the Li-ion diffusion distance and increase access to active sites. Theoretical studies[54,55] have also been employed to understand further the Li-ion insertion mechanism and transfer pathways at the anode. This section will introduce the most recent investigations of COFs as anode materials. Some reported critical parameters of these COF batteries are summarized in **Table 1**.

2.1.1. Highly Conjugated and Redox-Active COFs as Anode

Conjugated structures feature a backbone chain of alternating double and single bonds and a delocalized electron system. Currently, highly conjugated COFs have been designed by many researchers and used as anode materials in LIBs. In 2005, Yang et al.[47] reported the application of highly conductive 2D COFs composed of porphyrin and 4-thiophenephenyl moieties as anode materials in LIBs (TThPP COF in **Figure 3**a). The uniform, large-area polymer anode films were directly prepared by in situ chemical oxidative polymerization of meso-tetrakis(4-thiophenephenyl) porphyrin on copper foil surface. The uniform COF films were comprised of many flat nanosheets and showed superior in-plane conductivity (2.38×10^{-4} Sm^{-1}) compared to most organic electrodes, which typically have conductivities below 10^{-5} Sm^{-1}.[41] The ordered alignment of 2D sheets facilitated the carrier transportation and Li-ion storage into layers and resulted in a high rate performance. It exhibited a reversible capacity (666 mAh g^{-1} at a current density of 200 mA g^{-1}) that was larger than graphitic[56] or other organic anodes.[57–63] At a current density of 1 A g^{-1}, The initial discharge and charge capacity reached 623 mAh g^{-1} and 401 mAh g^{-1}, respectively, and discharge capacity stabilized at 381 mAh g^{-1} after 200 cycles.

Bai et al.[43] prepared two fully conjugated COFs, N2-COF (Figure 3b) and N3 COF (Figure 3c), with high surface areas (1496 and 1142 m^2 g^{-1}, respectively). N2-COF and N3-COF have ordered stacking channels and features very small pore sizes (N2-COF ≈2.3 nm; N3-COF ≈1.6 nm). The ordered stacking enhanced Li-ion transport and electrolyte permeation. When the two COFs were applied as anode materials without any binders in LIBs with a metallic Li counter electrode in coin cells (2032), they showed discharge capacities of 735 and

Table 1. Performance summary of COF anodes.

Anode materials	COFs	Electrolyte	First charge-discharge (CC/DC/R)	Cycling stability (RC/R/CN)	Voltage vs Li/Li+/V	Ref.
Pure TThPP film	TThPP COF	1 M $LiPF_6$/EC/DMC(1:1,v/v)	401/623/1000	381/1000/200	0.005–3	[47]
Pure N2-COF without any binder	N2-COF	1 M $LiPF_6$/EC/DMC/DEC (1:1:1,v/v)	689/735/1000	600/1000/500	0.05–3	[43]
Pure N3-COF Without any binder	N3-COF	1 M $LiPF_6$/EC/DMC/DEC (1:1:1,v/v)	707/731/1000	593/1000/500	0.05–3	[43]
65 wt% PA-COF+25 wt% CB+10 wt% (PVDF)	PA-COF	1 M $LiPF_6$/EC/DMC/DEC (1:1:1,v/v)	267/321.9/1000	401.3/1000/500	0.01–3.5	[48]
65 wt% TB-COF+25 wt% CB+10 wt% (PVDF)	TB-COF	1 M $LiPF_6$/EC/DMC/DEC (1:1:1,v/v)	262.4/311.4/1000	379.1/1000/500	0.01–3.5	[48]
Cz-COF-1/acetylene black/sodium Alginate (5:3:2, w/w/w)	Cz-COF-1	1 M $LiPF_6$/EC/EMC/DMC (1:1:1 v/v)	≈400/≈390/200 Second cycle	236/200/400	0.005–3	[45]
Cz-COF-1/acetylene black/sodium Alginate (5:3:2, w/w/w)	Cz-COF-2	1 M $LiPF_6$/EC/EMC/DMC (1:1:1 v/v)	≈270/≈270/200 second cycle	≈158/200/400	0.005–3	[45]
DBA-COF 3/Super P/ PVDF (6:3:1, w/w/w)	DBA-COF 3	1 M $LiPF_6$/EC/DMC (1:1 v/v)	–/–/–	207/50/90	0.05–3	[44]
COF@CNT/acetylene black/ PVDF(8:1:1, w/w/w)	COF-LZU1	1 M $LiPF_6$/EC/DEC (1:1 w/w)	383/928/100	1021/100/500; 1536/100/500	0.005–3	[49]
TFPB-COF/CB/PVDF (8:1:1, w/w/w)	TFPB-COF	1 M $LiPF_6$/EC/DEC (1:1 w/w)	–/–/–	126/100/300	0.005–3	[53]
E-TFPB-COF/CB/PVDF (8:1:1, w/w/w)	TFPB-COF	1 M $LiPF_6$/EC/DEC (1:1 w/w)	1211/2046/100	968/100/300	0.005–3	[53]
E-TFPB-COF-MnO_2/CB/ PVDF (8:1:1, w/w/w)	TFPB-COF	1 M $LiPF_6$/EC/DEC (1:1 w/w)	1274/2423/100	1359/100/300	0.005–3	[53]
IISERP-CON2/CB/PTFE (7.5:2:0.5)	IISERP-CON2	1 M $LiPF_6$/EC/DMC (1:1 w/w) +2% FEC	≈160/340/100	790/100/1000	0.01–3	[50]
IISERP-CON3/CB/PTFE (7.5:2:0.5)	IISERP-CON3	1 M $LiPF_6$/EC/DMC (1:1 w/w) +2% FEC	≈170/230/100	580/100/1000	0.01–3	[50]
IISERP-COF7/CB/PTFE (7.5:2:0.5)	IISERP-COF7	1 M $LiPF_6$/EC/DMC (1:1 w/w) +2% FEC	≈240/≈240/100	200/100/1000	0.01–3	[50]
IISERP-COF8/CB/PTFE (7.5:2:0.5)	IISERP-COF8	1 M $LiPF_6$/EC/DMC (1:1 w/w) +2% FEC	≈160/≈160/100	130/100/1000	0.01–3	[50]
IISERP-CON1/CB/PTFE (7.5:2:0.5)	IISERP-CON1	1 M $LiPF_6$/EC/DMC (1:1 w/w) +2% fluoro ethylene glycol	≈750/2060/100	≈600/500/1000	0.01–3	[52]

Note: all of them are half cells by using lithium metal as counter electrode; ethylene carbonate = EC; dimethyl carbonate = DMC; ethyl methylcarbonate = EMC; diethyl carbonate = DEC; 1,3-dioxolane = DOL; dimethoxyethane = DME; Fluoroethylene carbonate = FEC; carbon black = CB; polyvinyl chloride = PVDF; CC = charge capacity, mAh g^{-1}; DC = discharge capacity, mAh g^{-1}; R = rate, mA g^{-1} or C; RC = reversible capacity, mAh g^{-1}; CN = cycling numbers.

732 mAh g^{-1} and charge capacities of 689 and 707 mAh g^{-1} at 1 C (or 1 A g^{-1}) for N2-COF and N3-COF, respectively. Each COF maintained excellent stability and showed a charge capacity of around 600 mAh g^{-1} after 500 cycles, 80% greater than the initial charge capacity. The long cycle stability was also reflected by the recovered capacity when the current density was reduced from 5 C to 2 C after many cycles.

A higher density of redox-active building blocks in conjugated COF structures can provide more lithium affinity sites and increase the potential capacity of batteries.[6,8–10,44,45] Researchers have developed versatile strategies to integrate more redox-active moieties[44,45] on each pore of COFs. Feng et al.[45] designed a bicarbazole-based redox-active monomer and successfully integrated it into highly crystalline COFs (Cz-COF1 and Cz-COF2, Figure 3d,e). The bicarbazole arrays around the pore provided a high density of redox-active sites. In contrast, open 1D pore channels facilitated the electrolyte and ion transport, making these two COFs ideal for energy storage applications. Cz-COF1 (Figure 3d) exhibited a charge storage capacity of 628 mAh g^{-1} at 100 mA g^{-1}, much higher than many POPs[64] and graphite.[56] Cz-COF1 (Figure 3d) also exhibited a capacity of 236 mAh g^{-1} after 400 cycles. Very recently, Wolfson et al.[44] reported COFs with dehydrobenzoannulene-based redox-active moieties (DBA-COF3, Figure 3f). The unique π-conjugated triangular-shaped macrocycles showed reversible redox performance, and the alkynyl ligands could successfully bind Li-ions, making it applicable for battery applications. However, it showed a lower capacity (207 mAh g^{-1} at 50 mA g^{-1}) and rate performance compared to other COF anodes.

Though researchers have made many efforts to design versatile COF structures to improve the anode electrochemical performance, a systematic understanding of the property-structure

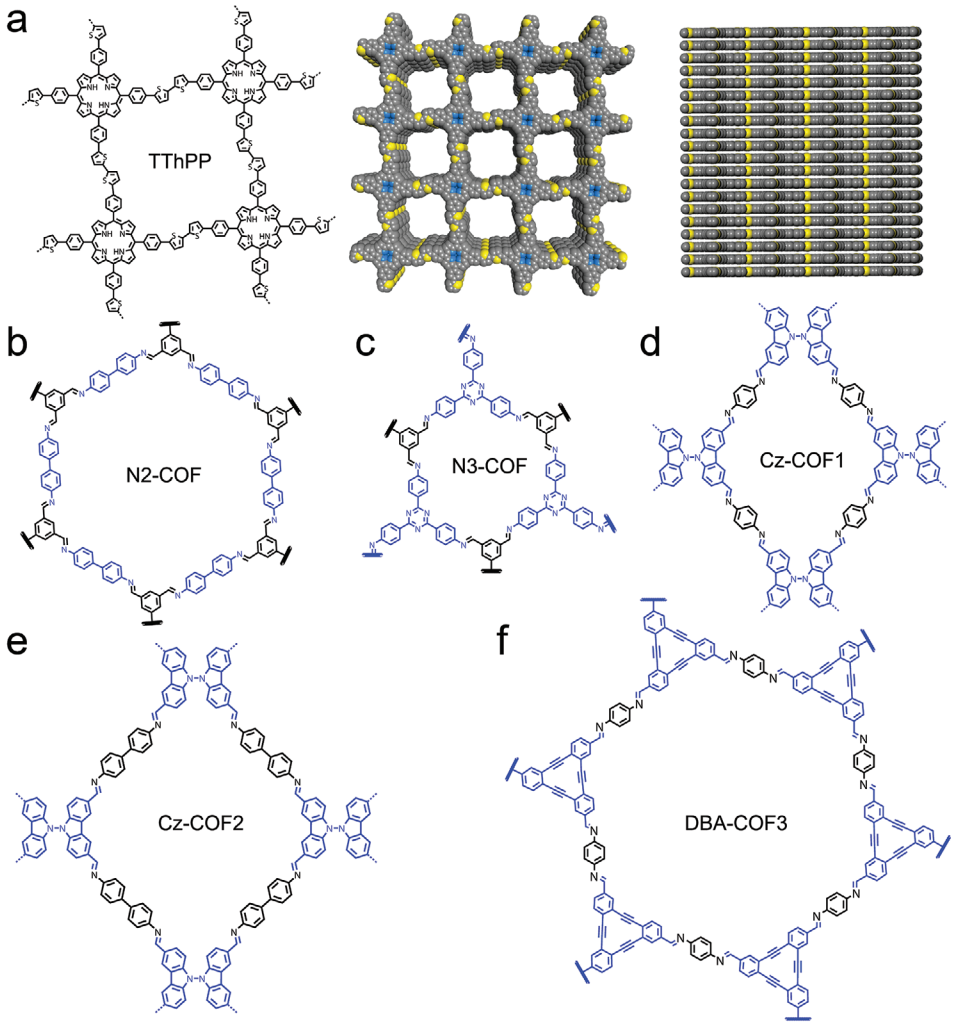

Figure 3. Different COF chemistries and structures studied as anode materials. a) TThPP COF and its top view and side view. b) N2-COF c) N3-COF. d) Cz-COF1 e) Cz-COF2. f) DBA COF3.

relationship and more molecular design strategies to increase the redox-active sites in the COF skeletons are still needed. It is crucial to study the electrochemical behavior of different conjugated COFs by systematically altering structural and chemistry variables. To increase the redox-active site density, the introduction of redox-active functionalities in each COF monomer may serve as a possible solution. Alternatively, the introduction of functionalized side chains with redox-active sites can also increase the energy density.

2.1.2. Incorporation with Conductive Carbons

Organic materials suffer from poor conductivity compared to carbon-based materials and inorganic materials. This can be addressed by blending them with carbon-based materials such as CNTs, graphene, or other commercial conductive carbons. Both physical blending and in situ growth have been applied as effective approaches. Physical blending is simple and straightforward. The active materials are usually mixed with carbon black as a conductive agent and polyvinyl chloride (PVDF; polyvinylidene fluoride) binder through stirring in appropriate solvents like *N*-methyl pyrrolidinone. Super-P conductive carbon and acetylene black are most widely used, and the weight percentage of these carbon additives usually ranges from ≈10–30 wt%. However, the interfacial charge transport barrier existed in electrode samples prepared by physical blending though the electron conductivity can be improved.

Another strategy that is widely explored for both COF anodes[49,65] and cathodes[66–69] is to grow the COFs in the presence of CNTs, graphene, or reduced graphene oxide (rGO) (**Figure 4**a,b). Through in situ growth, COFs can bind with carbon materials through chemical interactions, which reduce the barrier for interfacial charge transport and enhance electron mobility.

For example, Wang and coworkers[49] achieved impressive charge storage capacities by in situ growth of COF-LZU on CNTs (1.4:1, w/w) (Figure 4c–e), which exhibited a high reversible capacity of 1021 mAh g^{-1} after 500 cycles at 100 mA g^{-1} (Figure 4e). The capacity first decreased to ≈230 mAh g^{-1} in

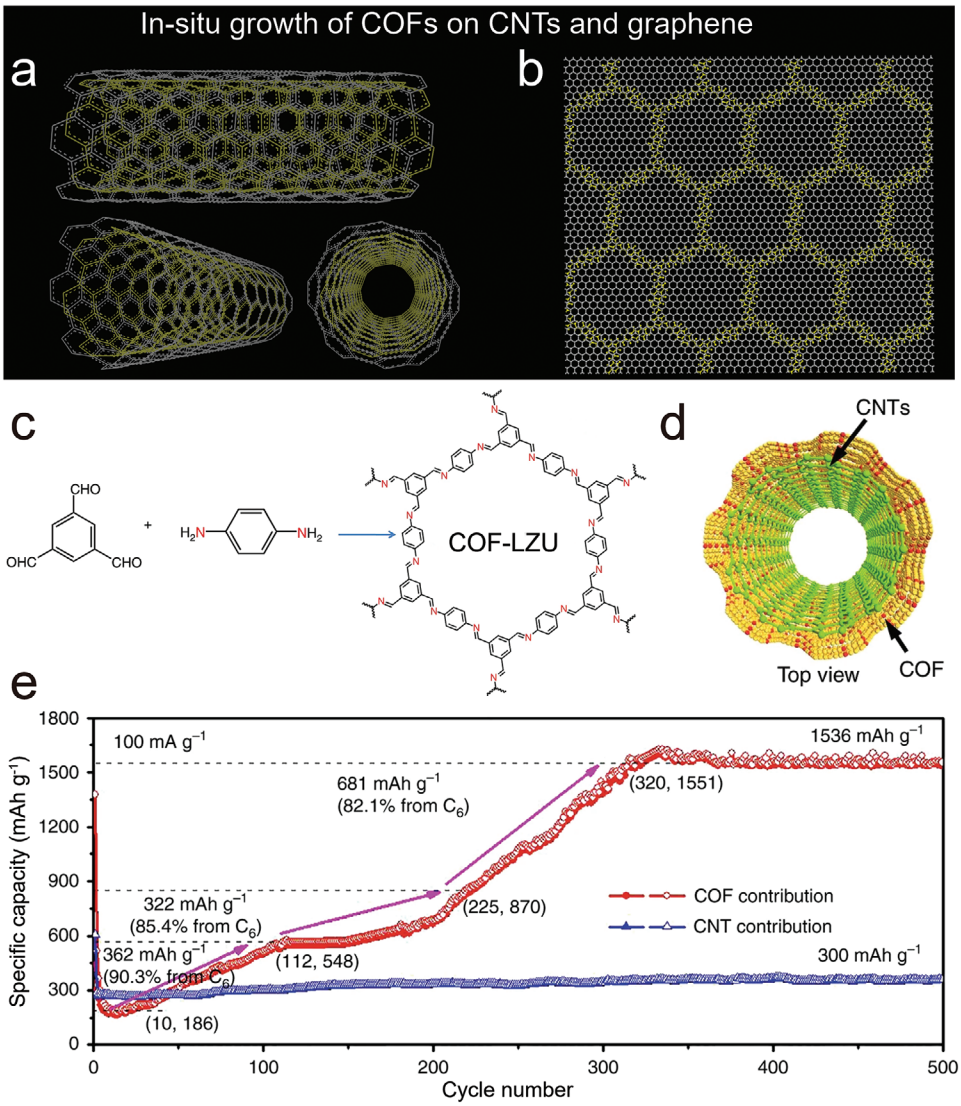

Figure 4. In situ growth of COFs on a) CNTs and b) graphene. c) Diagrams for synthesis of COF-LZU. d) Top view schematics of COF@CNT. e) Cycling performance of COF@CNT. c–e) Reproduced with permission.[49] Copyright 2018, Nature Publishing Group.

the initial ten cycles, then increased to 443 mAh g^{-1} from the tenth to 112th cycle, subsequently increased to ≈600 mAh g^{-1} over the 112th to 225th cycle, and finally rapidly increased to 1021 mAh g^{-1} from the 225th to 500th cycles and maintained this capacity without further degradation (Figure 4e). CNTs played a significant role in improving the electrochemical performance of this anode. First, CNTs enhanced the electron conductivity of COFs through chemical binding and π–π interaction. Second, few-layer COFs can be produced due to the in situ separation by CNTs, thus exposing more redox-active sites.

While in situ growth is promising, it is difficult to control the uniformity of COFs on the conductive carbons. COFs are typically synthesized under solvothermal conditions without stirring, so the carbon materials precipitate in the reaction solvent and lead to the non-uniform growth of COFs on them. Furthermore, these carbon materials usually have a low dispersity in COF synthesis solution and have low interactions with COF functionalities. Therefore, it is important to improve the solvent dispersity of carbon materials and chemical interactions with COFs through surface modification techniques such as the introduction of NH_2, CHO, and COOH functionalities. Microwave reactions can also serve as an effective approach to ensure the homogeneous growth of COFs on carbon materials since microwave reactions produce highly crystalline and porous COFs and enable homogeneous dispersion of carbon materials in solution simultaneously.

2.1.3. Exfoliation of Bulk COFs into Nanosheets

Another challenge of the COF anodes is to overcome the sluggish lithium diffusion caused by multiple stacking layers. The stacking of COF sheets increases the Li-ion insertion distance and leads to poor lithium diffusion kinetics. This multilayer stacking can also block redox-active sites. Exfoliation of bulk COFs into few-layer nanosheets can increase the exposed

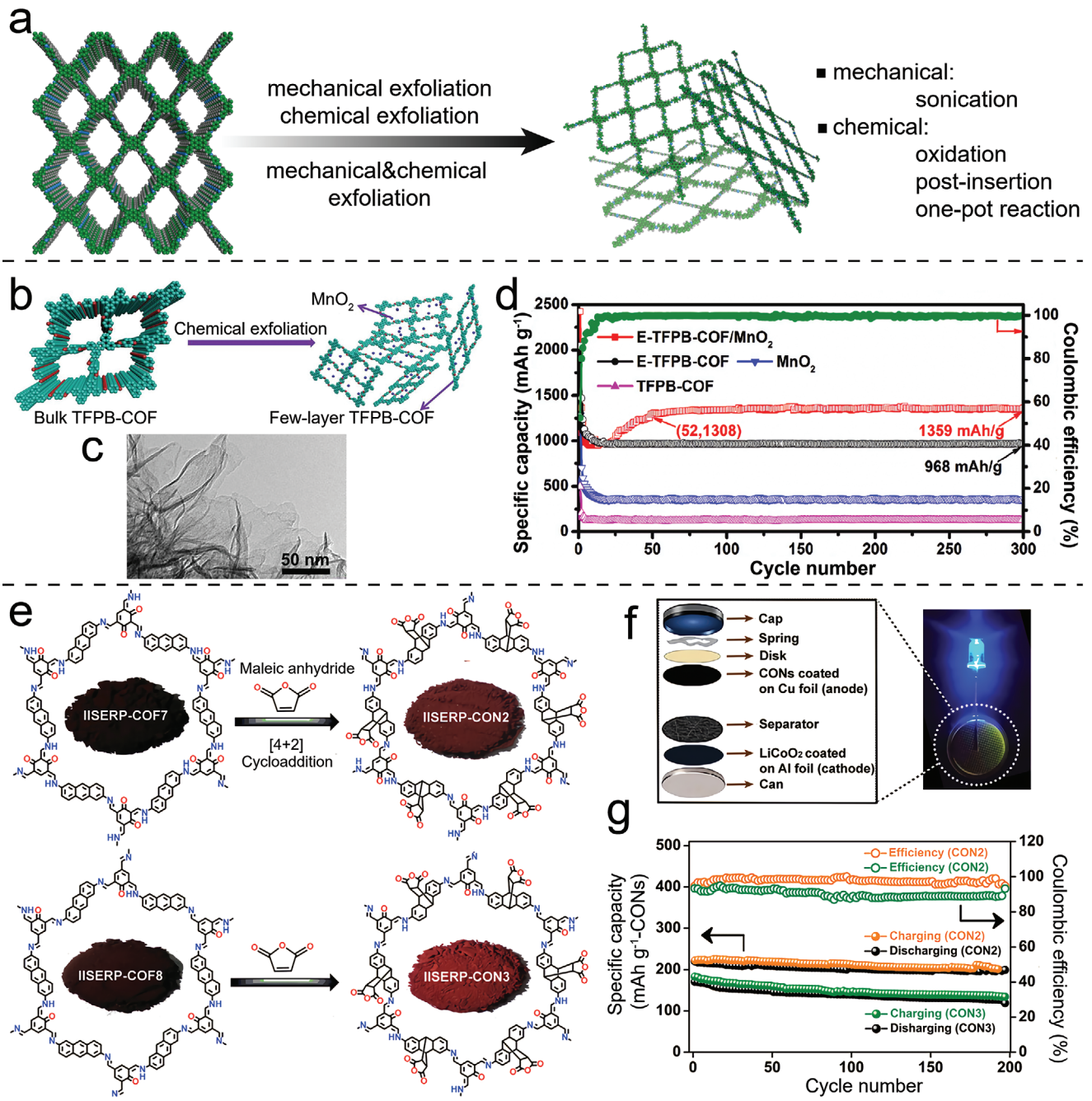

Figure 5. a) Schematic showing multiple approaches to exfoliate bulk COFs into few-layer nanosheets. b) Chemical exfoliation synthesis of few-layer ETFPB-COF with MnO_2 particles from bulk COFs. c) High-resolution transmission microscopy graph of E-TFPB-COF/MnO_2. d) Cycle performance of TFPB-COF, ETFPB-COF, and ETFPB-COF/MnO_2. b–d) Reproduced with permission.[53] Copyright 2019, Wiley-VCH. e) Diagrams for synthesis of IISERP-CON2 and IISERP-CON3 from bulk COFs through Diels–Alder reaction. f) Assembly of full cells using CONs and $LiCoO_2$. g) Cycle performance of CONs. e–g) Reproduced with permission.[50] Copyright 2019, Wiley-VCH.

redox-active sites, reduce the lithium insertion distance, enhance the lithium transfer kinetics, and boost their electrochemical performance. Exfoliation of graphite into few-layer or single-layer graphene proves to be an effective strategy to improve the energy storage performance and has been widely investigated.[70] Similarly, researchers have managed to synthesize few-layer COF nanosheets (or called CONs)[50,52,53] from bulk COFs through multiple exfoliation methods to overcome the drawbacks of bulk materials (**Figure 5**a).

Chen et al.[53] synthesized a bulk TFPB-COF (Figure 5b) and then exfoliated it into few-layer nanosheets (ETFPB-COF, Figure 5b,c) through a strong oxidant intercalation process using $HClO_4$. They then produced an ETFPB-COF/MnO_2 composite through in situ reduction of $KMnO_4$ on ETFPB-COF

(Figure 5b). The presence of MnO_2 nanoparticles prevented the re-stacking and aggregation of ETFPB-COF nanosheets. The composite anode exhibited high capacity and long cycling stability due to the unique 2D few-layer structure and synergetic effect of COF and MnO_2 nanoparticles. The composite displayed an initial charge/discharge capacity of 2423 mAh g^{-1} and a reversible capacity of 1359 mAh g^{-1} after 300 cycles at 0.1 A g^{-1} (Figure 5d). The porous structure of COFs suppressed significant volume expansion and shrinkage during the charge and discharge process. Meanwhile, the few-layer 2D structure exposed more redox-active sites, shortened the Li-ion insertion distance, and facilitated their diffusion, leading to a higher capacity and shorter activation process compared to COF/CNT.[49]

Haldar et al.[50] exploited a chemical exfoliation method through post-insertion and successfully delaminated bulk COFs into few-layer CONs as anodic electrode materials. In detail, they first synthesized two bulk anthracene-based COFs (IISERP-COF7 and IISERP-COF8, see Figure 5e) and then utilized a thermal Diels–Alder reaction between anthracene moiety and maleic anhydride to exfoliate the black bulk COFs into brownish-red ultrathin CONs (CON2 and CON3, see Figure 5e) with a thickness ranging from 2 to 5 layers. COFs have relatively lower interlayer interactions and are much easier to be exfoliated compared to graphite, so the steric obstruction between layers generated by maleic anhydride could successfully expand layer distance, weaken the layer interactions, and thus assist the chemical exfoliation process. Maleic anhydride also introduced more redox-active carbonyl groups into COF structures and increased the theoretical capacity. When the CONs were applied as anode electrodes in a half cell with CON-$LiPF_6$-Li metal coin-cell configurations, they delivered a steady capacity of 790 mAh g^{-1} for IISERP-CON2 (see structure in Figure 5e) and 580 mAh g^{-1} for IISERP-CON3 (see structure in Figure 5e) after 280 cycles at 100 mA g^{-1}. After running for several cycles, the insertion of lithium into CONs occurred at very low potential (0–0.03 V) and contributed more current during this potential range. Furthermore, a full cell was fabricated by the assembly of CONs as anode and $LiCoO_2$ as cathode to evaluate the actual performance of CONs (Figure 5f). The potential window was set as E^0 +/− 0.5 V to ensure complete lithiation and delithiation. CON-2 and CON-3 exhibited specific capacities of 220 mAh g^{-1} with 92% capacity retention and 170 mAh g^{-1} with 68% capacity retention after 200 cycles, respectively (Figure 5g).

In addition to top-down strategies, bottom-up approaches are also effective in synthesizing few-layer nanosheets through the direct polycondensation of starting monomers. For example, Haldar et al.[52] found few-layer COFs could be synthesized through a self-exfoliation process if the interlayer π–π interactions are weak enough. They were able to prepare triazole-triformyl phloroglucinol-based ultrathin CONs in one pot under mild conditions without further post-exfoliation. As an anodic material in half cells, these CONs showed a specific capacity of 720 mAh g^{-1} at 100 mA g^{-1}, which was the highest among all self-standing non-graphite organic materials. After 100 cycles, it retained a capacity of ≈570 mAh g^{-1} at a current density of 1 A g^{-1}, and the half cell retained Coulombic efficiency of 98% after 1000 cycles. However, bottom-up approaches cannot be widely applied to a variety of COFs since this method highly depends on monomer chemistry. More general ways such as introduction of templating agents should be developed to expand the applicable scope of bottom-up approaches.

In summary, multiple exfoliation approaches, including mechanical exfoliations and chemical exfoliations, have been utilized in the synthesis of COF nanosheets for electrode applications. It is still challenging to scale up and synthesize a large amount of COF nanosheets using a straightforward approach. Post-synthetic exfoliation also damaged the crystallinity of COFs. So, it is essential to develop one-pot synthesis strategies that can be easily scaled up without sacrificing the crystallinity of COFs. Controlling the thickness of COF nanosheets through exfoliations is also challenging. Introduction of side functionalities on the pore channels of COFs that form steric hindrance and assist the exfoliation of interlayer sheets may serve as a possible solution.

2.2. COFs with Different Linkages as Cathode

Compared to anode materials, cathode materials play a more significant role in determining the specific capacity and working voltage of LIBs.[26,27,37] Graphite is the most widely used anode material and has a large theoretical capacity of 372 mAh g^{-1}.[25,26] By comparison, cathodes generally have much lower capacities (generally <200 mAh g^{-1}), representing a bottleneck in the improvement of LIB energy density.[23,26,27,37,38] Inorganic materials including $LiCoO_2$, olivine $LiFePO_4$, $LiMO_2$ (M: Ni, Co, Mn, etc.), and lithium-rich layered oxide $xLi_2MnO_3(1–x)LiMO_2$ (M: Ni, Co, Mn, etc.) are of significant interest for cathodes.[23,26,38] COFs are also extensively investigated, and current studies on COF cathode materials mainly focus on design carbonyl structures in COFs with different linkages and enhancement of conductivity by incorporation of carbon materials.[66–69,71,72] In this section, we comprehensively summarize the most recent applications of carbonyl-containing COFs with various linkages (boronate,[66] boroxine,[71] imine,[72] and imide[67–69]) as cathode materials (**Figure 6**). Strategies used in the anode section (e.g., incorporation with carbon materials, exfoliation, etc.) have also been applied in cathode materials and will be discussed in specific works. The critical parameters for the electrochemical performance of COF cathodes are summarized in **Table 2**.

The first generation of cathode COF materials is based on unstable boronate-linked and boroxine-linked COFs. In 2015, Jiang and coworkers[66] designed a redox-active, crystalline, mesoporous COF with boronate linkages and naphthalene diimide walls on CNT (DTP-ANDI-COF, see Figure 6a). Naphthalene diimide monomer experienced significant discharge capacity attenuation due to the monomer dissolution in the electrolyte. By comparison, DTP-ANDI-COF@CNTs demonstrated much higher stability and capacity due to the low solubility in the electrolyte, abundant porosity for electrolyte transportation, increased active site exposure, and higher electron mobility assisted by CNT. DTP-ANDI-COF@CNTs cathode achieved a capacity of 67 mAh g^{-1} and maintained a 100% Coulombic efficiency after 100 cycles, indicating an 82% utilization efficiency of redox-active sites in the DTP-ANDI-COF@CNTs

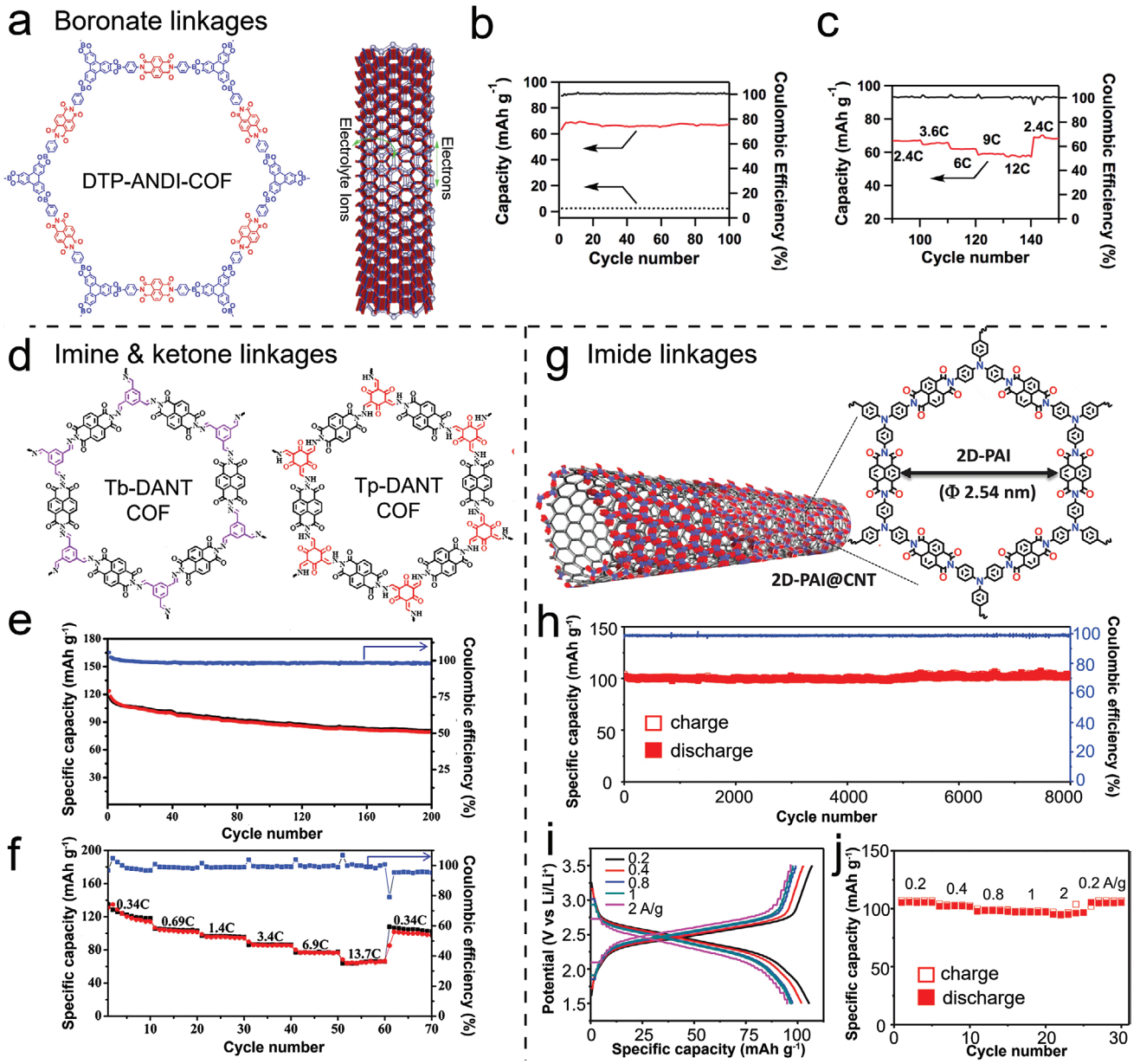

Figure 6. Development of COFs with increasingly stable linkages as cathode materials. a) DTP-ANDI-COF with boronate linkages and DTP-ANDI-COF@CNT composites. b) Cycling performance and c) rate performance of DTP-ANDI-COF@CNT. a–c) Reproduced with permission.[66] Copyright 2015, Nature Publishing Group. d) Tb-DANT COF with imine linkages and Tp-DANT COF with ketone linkages. e) Cycling performance of Tb–DANT-COF; f) rate capability and Coulombic efficiency of Tb–DANT-COF. d–f) Reproduced with permission.[72] Copyright 2016, Royal Society of Chemistry. g) Graphics of 2D-PAI@CNT. Electrochemical test for 2D-PAI@CNT: h) cycle performance, i) charge-discharge profiles, j) rate capacity. g–j) Reproduced with permission.[69] Copyright 2019, Wiley-VCH.

cathodes and a 100% utilization efficiency of electrons and ions involved in the oxidation and reduction reactions (Figure 6b). CNTs allowed for rapid charge and discharge with negligible hysteresis, and as a result, the cathode demonstrated a rapid charge and discharge potential. The cathode also demonstrated good rate performance at a high charge rate. For example, the capacity was 58 mAh g^{-1} at 12 C, representing an 85% retention of the capacity at 2.4 C (Figure 6c, red line). Yao et al.[13] designed a boroxine-linked COF with redox-active sites pyrene-4,5,9,10-tetraone. A cathode composed of 70% COF and 30% CNT without any binder exhibited a specific capacity of 198 mAh g^{-1}, only 24% capacity decrease at 1000 mAh g^{-1} compared to that at 100 mAh g^{-1}, and Coulombic efficiency of 99.6% after 150 cycles. In general, the specific capacities of bonoate-linked and boroxine-linked COFs are low compared to existing polymer cathodes.[39,73,74] Additionally, the long-cycle stability of these COF cathodes is limited due to the insufficient chemical stability of boronate or boroxine linkages in the electrolyte.

The stability of COF cathodes has to be improved to achieve longer recycling performance. To address this problem, the

Table 2. Summary table of COF cathode.

Cathode materials	COFs	Electrolyte	Initial capacity (CC/DC/R)	Cycling stability (RC/R/CN)	Voltage vs Li/Li+/V	Ref.
DTP-ANDI-COF	DTP-ANDI-COF	$LiPF_6$/EC+DMC (1:1, w/w)	–/42/200	21/200/30	1.5–3.5	[66]
DTP-ANDI-COF/CNT	DTP-ANDI-COF	$LiPF_6$/EC+DMC (1:1, w/w)	60/62/200	74/200/700	1.5–3.5	[66]
PPTODB/MWCNT	PPTODB	$LiPF_6$/EC+DMC (1:1, v/v)	–/–/–	198/20/150	1.5–3.5	[71]
Tp-DANT-COF	Tp-DANT-COF	1 M $LiPF_6$/EC+DMC/EMC (1:1:1, v/v/v)	78.9/93.4/200	72.8/200/600	1.5–4.0	[72]
Tb–DANT-COF	Tb–DANT-COF	1 M $LiPF_6$/EC+DMC/EMC (1:1:1, v/v/v)	135.4/144.4/50	80.1/500/300	1.5–4.0	[72]
PIBN-G	PIBN	1.0 M LiTFSI/DOL)/DME) (1:1, v/v)	–/242.3/1 C & –/206.7/5 C	208.1/1 C/300 & 182.3/5 C/300	1.5–3.5	[67]
PI-COF-1	PI-COF-1	1.0 M $LiPF_6$/DMC/EC/EMC (1:1:1 v/v/v)	84/85/14.2	–/–/–	1.5–3.5	[68]
PI-ECOF-1	PI-ECOF-1	1.0 M $LiPF_6$/DMC/EC/EMC (1:1:1 v/v/v)	105/112/14.2(0.1 C) second cycle	43/1 C/300	1.5–3.5	[68]
PI-ECOF-1	PI-ECOF-1	1 M LiTFSI/DOL/DME (1:1, v/v)	102/103/14.2(0.1 C) second cycle	72/1 C/300	1.5–3.5	[68]
PI-ECOF-1/rGO10 (10% rGO, w/w)	PI-ECOF-1	1 M LiTFSI/DOL/DME (1:1, v/v)	120/110/14.2(0.1 C) second cycle	83/1 C/300	1.5–3.5	[68]
PI-ECOF-1/rGO30 (30% rGO, w/w)	PI-ECOF-1	1 M LiTFSI/DOL/DME (1:1, v/v)	140/127/14.2(0.1 C) second cycle	90/1 C/300	1.5–3.5	[68]
PI-ECOF-1/rGO50 (50% rGO, w/w)	PI-ECOF-1	1 M LiTFSI/DOL/DME (1:1, v/v)	180/167/14.2(0.1 C) second cycle	102/1 C/300	1.5–3.5	[68]
PI-ECOF-2	PI-ECOF-2	1 M LiTFSI/DOL/DME (1:1, v/v)	118/103/14.2(0.1 C) second cycle	40/1 C/300	1.5–3.5	[68]
PI-ECOF-2/rGO	PI-ECOF-2	1 M LiTFSI/DOL/DME (1:1, v/v)	130/124/14.2(0.1 C) second cycle	67/1 C/300	1.5–3.5	[68]
2D-PAI	2D-PAI	1 M LiTFSI/DOL/DME (1:1, v/v)	NR	28.5/100/50	1.5–3.5	[69]
2D-PAI@CNT	2D-PAI	1 M LiTFSI/DOL/DME (1:1, v/v)	NR	104.4/100/8000	1.5–3.5	[69]

Note: All of them are half cells by using lithium metal as anode; ethylene carbonate = EC; dimethyl carbonate = DMC; ethyl methylcarbonate = EMC; lithium bis (trifluoromethane) sulfonimide = LiTFSI; 1,3-dioxolane = DOL; dimethoxyethane = DME; CC = charge capacity, mAh g^{-1}; DC = discharge capacity, mAh g^{-1}; R = rate, mA g^{-1} or C; RC = reversible capacity, mAh g^{-1}; CN = cycling numbers.

second-generation COF cathode materials with imine or ketone linkages were proposed.[72] For example, Yang et al.[72] designed an amine monomer containing naphthalene diimide and prepared two highly crystalline imine- and ketone-linked COFs (Tp–DANT-COF and Tb–DANT-COF, see Figure 6d). The conjugated backbones and regular pores facilitated the ion transport, and strong covalent linkages helped avoid the dissolution of redox-active moieties. Hence, these two COFs exhibited higher specific capacity and improved cycling stability compared to boronate- and broxine-linked COFs. Tb–DANT-COF delivered an initial discharge capacity (123.7 mAh g^{-1}) and retained a discharge capacity after 200 cycles (Figure 6e). Tb–DANT-COF also exhibited good rate performance. The specific discharge capacities were 118.1, 101.7, 94.4, 85.4, 76.8, and 66.6 mAh g^{-1} at current rates of 0.34, 0.69, 1.4, 3.4, 6.9 and 13.7 C, respectively. The discharge capacity recovered gradually when the current rates suddenly decreased to 0.69 C (Figure 6f).

The third generation of COF cathode materials is based on imide-linked COFs with greatly improved stability compared to imine- or boronate- or broxine-linked COFs. For example, Luo et al.[67] designed a microporous imide COF featuring abundant carbonyl groups (10 redox-active sites in each repeat unit). After blending with graphene, it exhibited a capacity of 271 mAh g^{-1} with fast kinetics and long cycle stability due to the sufficient utilization of carbonyl groups and enhanced electron and Li-ion mobility. Wang et al.[68] also incorporated rGO sheets with imide COFs to improve the conductivity. The bulk COFs were further exfoliated into few-layer nanosheets to expose the redox-active sites fully. The bulk imide COF/rGO displayed a capacity of 85 mAh g^{-1} (60% of theoretical capacity), whereas the few-layer imide COF/rGO showed a higher capacity of 112 mAh g^{-1} (79% of theoretical capacity). The few-layer imide COF/rGO cathode retained a nearly constant capacity after 300 cycles, and their Coulombic efficiencies kept almost 100%. A milestone in the development of imide COF cathodes was a 2D polyacrylimide COF grown on CNT (2D-PAI@CNT, Figure 6g) reported by Feng and coworkers.[69] It achieved extremely long stability without capacity fading after 8000 cycles (Figure 6e). The capacity of 2D-PAI@CNT was similar to the capacitor and had less relevance with the current (Figure 6i,j). The fast transportation of Li-ions and electrons within the 2D-PAI@CNT electrodes ensured the charge-discharge curves to keep a similar shape without apparent polarization (Figure 6i).

In summary, COF cathode materials have evolved from those with unstable linkages (boronate, broxine) to those with more stable linkages (imide). Stabler linkages hinder the dissolution of COFs in electrolytes and enormously enhance their recycling stability. However, imide-linked COFs are very difficult to synthesize due to the harsh reaction conditions, including high temperature (180–250 °C) and long reaction time.[69,75,76] To date, only a few imide COFs have been reported.[69,75–77] It is necessary to develop more straightforward synthesis approaches for imide COFs and enrich the imide COF library. Developing COFs with other stable linkages like polyarylether linkages,[78] amide linkages,[79] oxazole linkages,[80] and thiazole linkages[80,81] can also serve as possible solutions.

2.3. Electrolyte

The electrolyte is another crucial component of an electrochemical battery. The electrolyte conducts ions between anode and cathode, but it is insulative to electrons.[23,28–32,38] Currently, liquid electrolytes are mostly used in LIBs, such as $LiPF_6$ combined with ethylene carbonate (EC) and dimethyl carbonate (DMC).[28,29,31,32] However, many intrinsic drawbacks exist in liquid electrolytes. First, liquid electrolytes have caused many safety concerns due to their low voltage windows and flammability, especially under high power operations or in large-size batteries.[28,29,31,82] Second, dissolution of active materials and side reactions often occur in liquid electrolytes, which deactivates the electrode materials and decreases the cycle stability and rate performance.[28–31] Third, liquid electrolytes usually have low lithium transport numbers around 0.5.[28–31]

Solid-state electrolytes (SSEs) can avoid the above issues and show a promising future in battery applications. Chalcogenides and solid-state polymers are commonly used as SSEs.[31] Chalcogenides are expected to have fast ion conductivities exceeding 10^{-2} S cm^{-1} due to the large size and high polarizability of chalcogenide ions. However, chalcogenides suffer from low energy densities due to their high molecular weights.[31,83] Solid-state polymers composed of all-light elements, such as polyethylene oxide (PEO) or polyethylene glycol (PEG), exhibit high chemical and thermal stability, so they are also commonly used as SSEs.[31,32] However, many solid-state polymers only have very low lithium transfer numbers (≈0.2–0.5) since most Li-ion transportations are facilitated by the swelling of polymer chains.[31,32,84]

COFs have been extensively investigated as solid electrolytes due to their ease of functionality and pore structure tunability.[82] Various strategies have been employed to enhance the Li-ion conductivity, reduce the activation energy, and improve Li^+ transfer numbers of COF SSEs.[17,18,84–91] This section will summarize the investigations on COF electrolytes to date, including ionic COFs, pore decorations, pore channel alignment, and COFs as artificial solid electrolyte interfaces (SEI). The key parameters to evaluate SSEs, including Li-ion conductivity, Li^+ transfer numbers, and activation energy, are summarized in **Table 3**.

2.3.1. Ionic COFs as SSEs

The introduction of ionic scaffolds in the structure of polymers can increase the dielectric constant of the materials and screen Coulombic interactions more effectively. Therefore, ionic functionalities can produce more free mobile ions and improved Li^+ conductivity. The incorporation of ionic functionalities in COFs has also been implemented as an effective approach to enhance Li^+ transport. In 2015, Zhang and coworkers[85] synthesized an ionic spiroborate-linked COF (ICOF-1, **Figure 7**a) and employed the Li^+ decorated ionic COF (ICOF-2, Figure 7a) as SSEs for the first time. ICOF-2 and PVDF composite films (2:1, w/w) were soaked in propylene carbonate (PC) and used as SSE. It exhibited a conductivity of 3.05×10^{-5} S cm^{-1} at room temperature without any contribution from PVDF or PC. ICOF-2 SSE also possessed a favorable activation energy (0.24 eV atom^{-1}) and Li^+ transfer number (0.80 ± 0.02). Similarly, Wang and coworkers[86] designed and synthesized a 3D spiroborate-linked anionic COF constructed by γ-cyclodextrins (γCD) and trimethyl borate ($B(OMe)_3$) (see CD-COFs in Figure 7b) through microwave-assisted solvothermal reactions. High porosity, flexible building blocks, and anionic feature of the CD-COFs led to excellent Li^+ conductivity. When they were employed as SSE after being immersed in a 1.0 M solution of $LiPF_6$ in EC and DMC with a volume ratio of 1:1 for 12 h twice and pressed into pellets, it displayed activation energy of 0.26 eV and Li^+ conductivity of 2.7×10^{-3} S cm^1 at 30 °C. Chen et al.[87] applied a cationic COF nanosheet (Figure 7c) as a SSE instead of using the bulk ionic COFs. Li-CON-TFSI (TFSI = bis (trifluoromethane) sulfonimide) SSE was synthesized through Schiff-base polycondensation (Step I, Figure 7c), replacement of Cl^- by $TFSI^-$ through ion-exchange with lithium bis (trifluoromethane) sulfonimide (LiTFSI) to produce CON-TFSI (Step II, Figure 7c), and incorporation with LiTFSI salt to produce Li-CON-TFSI (Step III, Figure 7c). Dry Li-CON-TFSI powder sample was directly pressed into pellets without using any solvent or plasticizers and tested using electrochemical impedance spectroscopy (EIS) at different temperatures. Li-CON-TFSI displayed a conductivity of 5.74×10^{-5} S cm^{-1} at 30 °C and 2.09×10^{-4} S cm^{-1} at 70 °C. It also showed comparable activation energy of 0.34 eV atom^{-1} as other reported COFs.[85,86] However, the Li^+ transfer number (0.61 ± 0.02) was relatively low.

Currently, only a low diversity of ionic COFs exists due to the limited quantities of ionic monomers. To design new ionic monomer structures that can interact with Li-ions may expand the application scope of ionic COFs. The relationship between Li-ion mobility and different ionic species is unclear and yet to be uncovered through systematic experimental and theoretical studies.

2.3.2. Pore Wall Decoration

Pore wall decoration is another effective approach to functionalize COFs and improve their electrolyte performance. Functional moieties can be either precisely predesigned in COF monomers or introduced into the COF skeleton through post-synthetic reactions. PEO-based electrolytes are attractive for LIBs due to their high energy density and compatibility with Li-ions.[17,31,32] Furthermore, PEO functionalities can provide high structural dynamics and high concentrated ion hopping sites for Li^+ motion.[17,31,32,84] Therefore, researchers have implemented PEO in COF structures to improve their ion conductivity.[17,18,84] Jiang and coworkers[17] first compared the electrolyte performance between a COF without PEO side chains and a COF with PEO side chains (TPB-BMTP-COF, see **Figure 8**a). The two COFs were further incorporated with Li^+ through solution diffusion of $LiClO_4$ and produced lithium inserted COFs. The lithium inserted COFs without PEO showed high activation energy (0.96 eV atom^{-1}) and low Li^+ conductivity (1.36×10^{-7}, 6.74×10^{-7}, and 5.37×10^{-6} S cm^{-1} at 40, 60, and 80 °C, respectively). However, the lithium inserted COFs with PEO side chains displayed a decreased activation energy (0.87 eV atom^{-1}) and improved Li^+ conductivity (6.04×10^{-6}, 2.85×10^{-5}, and 1.66×10^{-4} S cm^{-1} at 40, 60, and 80 °C, respectively). By comparison, composites

Table 3. Summary of COFs as solid-state electrolytes.

Pub year	COFs	Additives	t_{Li+}	σ (S cm^{-1})	E_a (eVatm^{-1})	Ref.
2015	ICOF-2 (with Li^+)	PVDF/PC	0.80 ± 0.02	3.05×10^{-5}@RT	0.24	[85]
2017	CD-COF (with Li^+)	$LiPF_6$/EC/DMC	NR	2.7×10^{-3}	0.26	[86]
2018	Li-CON-TFSI	LiTFSI	0.61 ± 0.02	5.74×10^{-5}@30 °C; 2.09×10^{-4}@70 °C	0.34	[87]
2018	Li^+@TPB-DMTP-COF	$LiClO_4$	NR	1.36×10^{-7} @40 °C	0.96	[17]
2018	Li^+@TPB-BMTP-COF	$LiClO_4$	NR	6.04×10^{-6}@40 °C	0.87	[17]
2018	Li^+&PEO@TPB-DMTP-COF	$LiClO_4$	NR	7.93×10^{-5} @40 °C	0.30	[17]
2019	Li^+@TPB-TP-COF	$LiClO_4$	NR	3.25×10^{-9}@40 °C;	NR	[18]
2019	Li^+@TPB-DMTP-COF	$LiClO_4$	NR	1.36×10^{-7} @40 °C	0.96	[18]
2019	Li^+@$[TEO]_{0.33}$-TPB-DMTP-COF	$LiClO_4$	NR	7.77×10^{-6}@40 °C	0.78	[18]
2019	Li^+@$[TEO]_{0.5}$-TPB-DMTP-COF	$LiClO_4$	NR	1.31×10^{-5}@40 °C	0.68	[18]
2019	Li^+@TPB-BMTP-COF	$LiClO_4$	NR	6.04×10^{-6}@40 °C	0.87	[18]
2019	Li^+@$[TEO]_{0.33}$-TPB-BMTP-COF	$LiClO_4$	NR	8.43×10^{-6}@40 °C	0.82	[18]
2019	Li^+@$[TEO]_{0.5}$-TPB-BMTP-COF	$LiClO_4$	NR	5.51×10^{-6}@40 °C	NR	[18]
2019	Li^+@$[TEO]_1$-TPB-BPTA-COF	$LiClO_4$	NR	9.04×10^{-7}@40 °C	NR	[18]
2019	COF-PEO-9-LiTFSI	LiTFSI	NR	0.12×10^{-3} @100 °C; 1.3×10^{-3} @200 °C; 7.8×10^{-3} @300 °C	NR	[84]
2019	COF-PEO-3-Li	LiTFSI	NR	9.72×10^{-5}@200 °C	NR	[84]
2019	COF-PEO-6-Li	LiTFSI	NR	3.71×10^{-4}@200 °C	NR	[84]
2019	COF-PEO-9-Li	LiTFSI	NR	1.33×10^{-3}@200 °C	NR	[84]
2019	PEG-Li^+@EB-COF-ClO_4	PEG; $LiClO_4$	0.60	1.93×10^{-5}@30 °C; 1.08×10^{-3}@100 °C; 1.78×10^{-3}@120 °C;	0.21	[88]
2019	PEG-Li^+@CD-COF-Li	PEG; $LiClO_4$	0.20	2.60×10^{-5}@30 °C; 1.30×10^{-4}@120 °C;	0.17	[88]
2019	PEG-Li^+@COF-300	PEG; $LiClO_4$	0.44	1.40×10^{-6}@30 °C; 9.11×10^{-5}@120 °C;	0.20	[88]
2019	PEG/Li^+/EB-COF-ClO_4	PEG; $LiClO_4$	NR	6.80×10^{-7}@30 °C;	NR	[88]
2019	PEG-Li^+@COF-5	PEG; $LiClO_4$	0.40	3.60×10^{-8}@30 °C; 3.49×10^{-5}@120 °C;	0.35	[88]
2019	Li^+@CD-COF-Li	$LiClO_4$	NR	7.81×10^{-7}@120 °C;	NR	[88]
2019	H-ImCOF and $LiClO_4$	$LiClO_4$, ≈20 wt% PC	0.21	4.0×10^{-5}@RT	NR	[89]
2019	H-Li-ImCOF	n-BuLi, ≈20 wt% PC	0.88	5.3×10^{-3}@RT	0.12	[89]
2019	CH_3-Li-ImCOF	n-BuLi, ≈20 wt% PC	0.93	8.0×10^{-5}@RT	0.27	[89]
2019	CF_3-Li-ImCOF	n-BuLi, ≈20 wt% PC	0.81	7.2×10^{-3}@RT	0.10	[89]
2019	TpPa-SO_3Li	LiOAc	0.90	2.7×10^{-5} @RT	0.18	[90]
2016	COF-5	$LiClO_4$	NR	2.6×10^{-4} @RT	0.37 ± 0.04	[91]
2016	TpPa-1 COFs	$LiClO_4$	NR	1.5×10^{-4} @RT	NR	[91]
2019	PVDF/S-COF-1	20 wt% COF additives	0.46	1.9×10^{-4} @RT	NR	[96]
2019	PVDF/H-COF-1@5	20 wt% COF additives	0.61	2.2×10^{-4} @RT	NR	[96]
2019	PVDF/H-COF-1@10	20 wt% COF additives	0.71	2.5×10^{-4} @RT	NR	[96]

Note: propylene carbonate (PC); ethylene carbonate (EC) and dimethyl carbonate (DMC).

prepared by physically mixing COFs without PEO side chains, $LiClO_4$, and PEO (average molecular weight Mn = 400) exhibited a much lower conductivity and thermal instability, indicating that covalent integration of oligo(ethylene oxide) chains on the pore walls was essential for reaching a stable polyelectrolyte interface and thus achieving stable performance. Jiang and coworkers further designed a series of COFs with varied densities of polyelectrolyte side chains on the hexagonal backbones.[18] They discovered that polyelectrolyte chains on the pore walls of COFs could significantly promote ion motion. Still, a higher

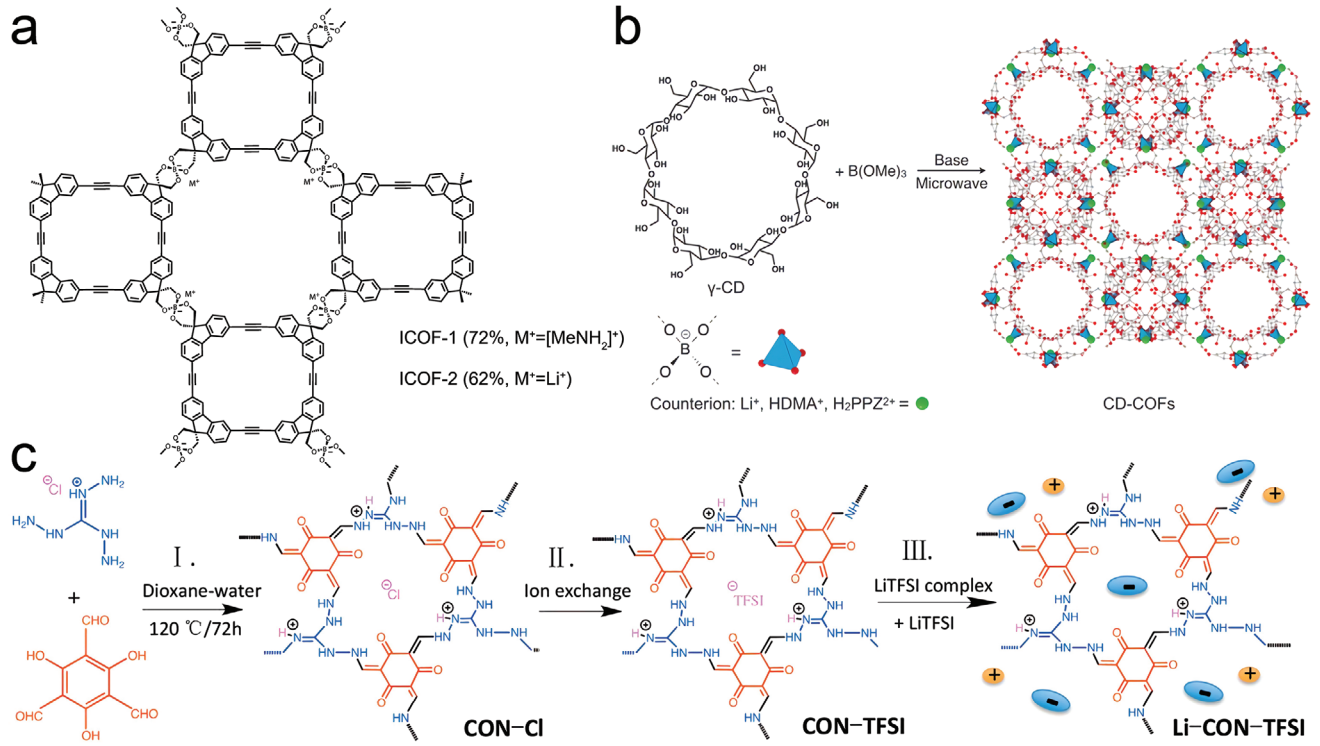

Figure 7. a) Structures of ICOF-1 and ICOF-2. Reproduced with permission.[85] Copyright 2016, Wiley-VCH. b) Diagrams for synthesis of CD-COFs. Reproduced with permission.[86] Copyright 2017, Wiley-VCH. c) Diagrams for three-step synthesis of Li-CON-TFSI. Reproduced with permission.[87] Copyright 2018, American Chemical Society.

concentration of polyelectrolyte chains above a threshold would lead to a significant decrease in pore volume and low loading of ion species. It is vital to control the concentration of polyelectrolyte chains and compromise between enhanced ion transport and decreased pore volume.

Horike and coworkers[84] also incorporated flexible, bulky, and glassy PEO moieties with different lengths (PEO-3, PEO-6, PEO-9) into hydrazone-linked COFs (COF-PEO-*x*, *x* = 3,6,9, see Figure 8b). PEO chains were predesigned in the hydrazide monomers rather than introduced through post-synthetic reactions to ensure a high loading. They found that increased length of PEO chains would decrease the crystallinity and internal surface area of COFs. To test the Li^+ conductivity, COF-PEO-*x* were incorporated with lithium bis (trifluoromethane) sulfonimide (LiTFSI) to form COF-PEO-*x*-Li samples. The Li^+ conductivity increased with the PEO length, and the conductivities of COF-PEO-3/6/9-Li at 200 °C were 9.72×10^{-5}, 3.71×10^{-4}, and 1.33×10^{-3} S cm^{-1}, respectively. However, the all-solid-state battery assembled using COF-PEO-9 as electrolyte showed poor stability and relatively low capacity. The actual application of COF SSEs still needed improvement.

Another effective molecular engineering strategy to improve Li^+ conductivity of solid-state COF electrolyte is integration of PEG functionalities (see Figure 8c). High-molecular-weight (weight average molecular weight, M_w) PEO decreases the crystalline regions and consequently limits ionic conductivity (≈10^{-7} S cm^{-1} at room temperature).[88] However, lower-molecular-weight PEG has high chain dynamics and can assist ion conduction.[88] In a work reported by Wang and coworkers,[88] they incorporated PEG units into anionic, neutral, or cationic COFs to accelerate Li^+ conduction (see Figure 8c). Instead of complicated chemical integration of PEG chains on the backbones, PEG-Li^+@COFs (Figure 8c) were simply prepared by immersing COFs in an acetonitrile solution of PEG and $LiClO_4$ followed by complete evaporation of the solvent. PEG could be confined in the pore channels of COFs rather than just adsorbed on the surface. Li^+ conductivity test revealed that the anionic COF (PEG-Li^+@CD-COF, Figure 8c) had a very low Li^+ transfer number (0.2) and low Li^+ conductivity. In contrast, neutral COFs (PEG-Li^+@COF-5 or COF-300, Figure 8c) and a cationic COF (PEG-Li^+@EB-COF-ClO_4, Figure 8c) exhibited higher Li^+ conductivity due to the enrichment of ion hopping pathways. Particularly, PEG-Li^+@EB-COF-ClO_4 (Figure 8c) offered a Li^+ transfer number of 0.6, which was higher than other COFs studied. It also displayed low activation energy of 0.21 eV and high Li^+ conductivity of 1.78×10^{-3} S cm^{-1} at 120 °C. This conductivity was ultrahigh among all polymeric crystalline porous materials based on all-solid-state conductors without any residue solvents. The critical parameters of other COF-derived electrolytes are summarized in Table 3.

Other functionalities such as imidazolate and sulfonate are also effective for enhancing the Li^+ conduction. For example, Zhang and coworkers[89] designed a series of ionic COFs with imidazolate decorated pore channels (H-ImCOF, CH_3-ImCOF, CF3-ImCOF, see Figure 8d). Li^+ encapsulated COFs (H-Li-ImCOF, CH_3-Li-ImCOF, CF_3-Li-ImCOF, Figure 8d) were prepared by stirring Im-COFs in n-BuLi/hexane solution (1.6 M, 0.1 mL). These Li-ImCOFs exhibited excellent Li^+ conductivity

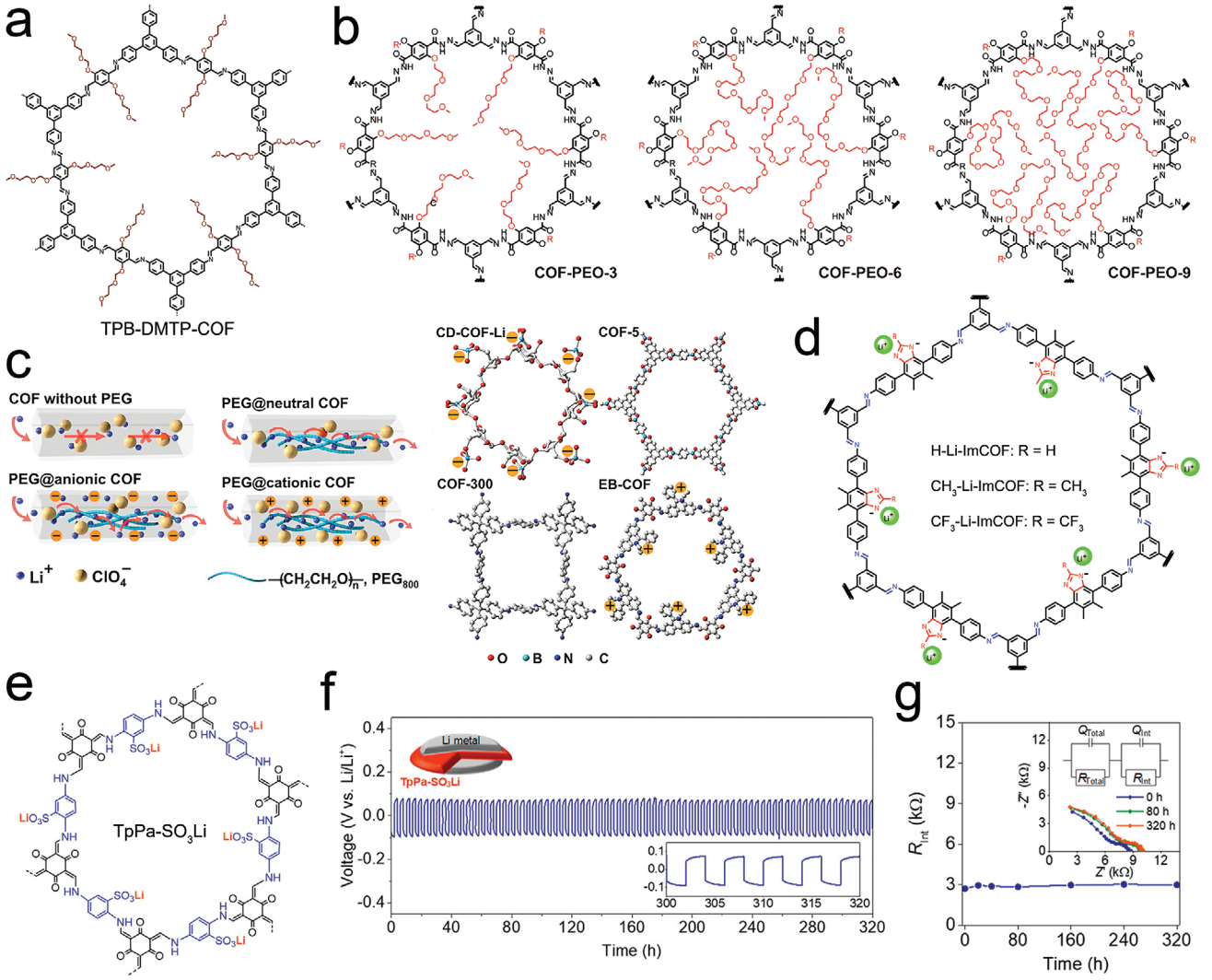

Figure 8. a) TBP-DMTP COF with PEO side chains. b) COF-PEO-3, COF-PEO-6, and COF-PEO-9. Reproduced with permission.[84] Copyright 2019, American Chemical Society. c) Schematics of PEG decorated COFs. Reproduced with permission.[88] Copyright 2019, American Chemical Society. d) Imidazolate decorated COFs. Reproduced with permission.[89] Copyright 2019, American Chemical Society. e) Chemical structure of TpPa-SO_3Li COF. f) Galvanostatic Li plating/stripping tests of the Li/Li symmetric cell composed of TpPa-SO_3Li. g) Electrochemical impedance spectroscopy (EIS) curves at cycling times of 0, 80, and 320 h. e–f) Reproduced with permission.[90] Copyright 2019, American Chemical Society.

(up to 7.2×10^{-3} S cm^{-1}), low activation energy (low to 0.10 eV $atom^{-1}$), and high Li^+ transfer number (0.81). CF_3-Li-ImCOF demonstrated the highest Li^+ conductivity due to the strong electron-withdrawing effect of CF_3 groups, which helped delocalize the negative charge of imidazolate anions and weakened the interactions between Li^+ and COF skeletons, thus promoting the ion motion and improved the Li-ion conductivity. Lee et al.[90] designed lithium sulfonated COF (TpPa-SO_3Li, Figure 8e) as a solvent-free, single Li^+ conductor. TpPa-SO_3Li possessed well-defined 1D pore channels, sulfonate tethered Li^+ on the edge of pores, and a high density of Li^+ inside the small pore channels, so it displayed a very high ion conductivity (2.7×10^{-5} S cm^{-1}), excellent Li^+ transfer number (0.9), and desired activation energy (0.18 eV $atom^{-1}$). A Li/Li symmetric cell was further fabricated by using TpPa-SO_3Li as the SSE and was repeatedly tested at 10 μA cm^{-2} for 4 h per cycle. The as-fabricated cell exhibited high Li plating/stripping stability and reliability. It did not show any significant decrease or irreversible fluctuation of overpotential after running more than 320 h (Figure 8f). Interfacial resistance (R_{Int}) of the cell did not increase appreciably with time, indicating a stable cyclability resulting from good interfacial stability between TpPa-SO_3Li electrolyte and Li metal electrodes (Figure 8g).

In summary, functionalization of the pore walls is an effective approach for enhancing the electrolyte performance of COFs. Functionalities including PEO, PEG, imidazolate, and sulfonate can improve the performance of COF SSEs. In the future, more effective functionalities should be designed to reduce the activation energy and enhance the Li-ion mobility. Furthermore, though the role of side functionalities has been elucidated, it is still necessary to understand the role of COF skeletons, including pore size, pore topology, and linkages.

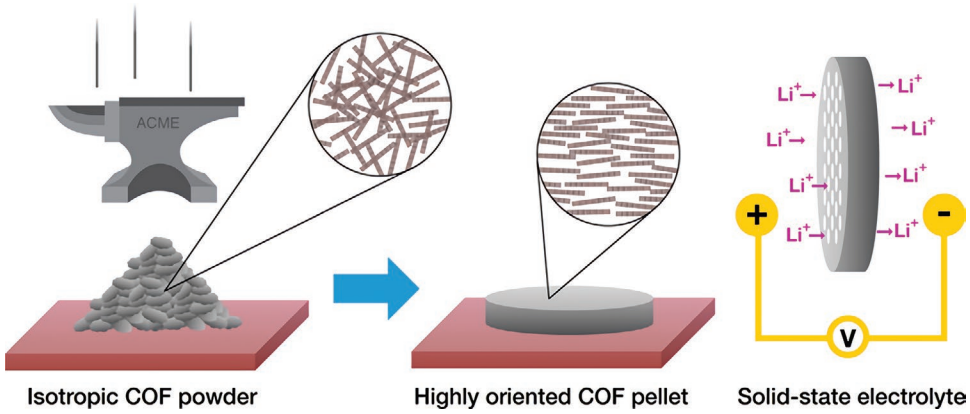

Figure 9. Schematics of mechanically shaped COFs for solid-state electrolyte. Reproduced with permission.[91] Copyright 2016, American Chemical Society.

2.3.3. Alignment of COF Pores

Alignment of COF pore channels can eliminate the ion transport pathway barriers and enhance ion mobility.[17,91] 2D COFs themselves have regular pore size and well-aligned vertical pore structures, but random stacking of COF particles may partially block COF cavities and hinder the rapid Li-ion mobility.[17,91] Uribe-Romo and coworkers[91] managed to shape the COF powders into pellets with good crystallographic alignment and fast ion conductivity through mechanical press (**Figure 9**). Mechanical press transformed the random orientation of COF powders into a preferred orientation where only 00*l* planes fulfilled the diffraction condition in parallel mode and only hk0 planes under perpendicular mode. This kind of preferred orientation applied to a variety of different COFs regardless of the linkages (boronate, boroxine, β-ketoenamine, triazine) or symmetries (hexagonal, tetragonal). Preferred orientation enabled the alignment of COF samples and thus alignment of cylindrical pores, which promoted the ion mobility and showed high application potential in LIBs. COF-5 incorporated with $LiClO_4$ was pressed into a pellet under 4 MPa uniaxial pressures and tested for EIS. The pellet showed an ionic conductivity of 2.6×10^{-4} S cm^{-1} at room temperature and activation energy of 0.37 ± 0.04 eV.

To align the COF pore channels, more reliable approaches should be developed. In situ growth of COFs on silicon or mica substrates may produce COF films with preferred orientation. In addition, interfacial polymerization of COF films between liquid/liquid or liquid/air interface may also produce COF films with a specific orientation, which provides reliable ways to synthesize COF films with aligned pore channels. Macroscale COF films with a certain thickness can be directly used as SSEs without any binders.

2.3.4. COF as Artificial SEI

Artificial SEI is extremely important for preventing Li-dendrite growth, which might impale SEI and battery separator, cause incident internal short circuit, and further trigger fires or explosions.[92–95] Stable, porous COFs are ideal materials for artificial SEI due to their high stability in the electrolyte, good mechanical property, and excellent ion transport selectivity. Meng and coworkers[92] in situ prepared a 10 nm thin layer of TAPB-PDA COF film on the Li metal electrode and successfully inhibited the Li-dendrite growth and stabilized Li plating/stripping (**Figure 10**a,b). Micropores of COFs allowed the effective penetration of electrolytes, selective transport of smaller ions (Li^+), and efficient block of larger ions like bis(trifluoromethane)sulfonimide ($TFSI^-$). Furthermore, COF thin films showed excellent mechanical strength (6.8 GPa) and successfully suppressed the irregular growth of Li-dendrite and inhibited the fracture of SEI.

Guo and coworkers[93] also prepared a β-ketoenamine-linked COF film as uniform artificial SEI on Li metal to accommodate anion-derived LiF grains in the microporous channels during charge-discharge cycling. The highly lithophilic COF incorporated with LiF served as a monolithic SEI and successfully restrained the volume expansion and dendrite growth of the Li metal anode. The coated Li anode demonstrated a lower activation energy (E_a = 0.10 eV), a higher Li^+ transfer number (0.79) and a larger ion conductivity (0.53 mS cm^{-3}) compared with bare Li metal anode (E_a = 0.14 V; Li^+ transfer number = 0.41; ion conductivity = 0.17 mS cm^{-3}).

Incorporation of COFs with commercial membranes can also act as effective artificial SEI. For example, CTF-LiF (CTF; covalent triazine framework) coated airlaid-paper (AP) was reported by Coskun and coworkers to have suppressed the Li-dendrite growth (see Figure 10c–f).[94] They first prepared a composite of CTF-1 and LiF through condensation of CTF-1 monomer and LiTFSI in one pot under ionothermal conditions[94] (Figure 10c). LiTFSI not only acted as a catalyst but a source of in situ-formed LiF particles. LiF particles effectively boosted the mechanical property and ion conductivity of CTF-1. As a result, CTF-LiF coated AP could successfully serve as an active Li hosting material for Li metal anode, and the synergistic effect of AP-CTF-LiF effectively suppressed the Li-dendrite growth.

2.4. COFs as Separator

Separators prevent the direct physical contact of anode and cathode to avoid the electrical short circuit.[33–36,97] They also serve as electrolyte reservoirs to enable ion mobility.[33,35,36,97]

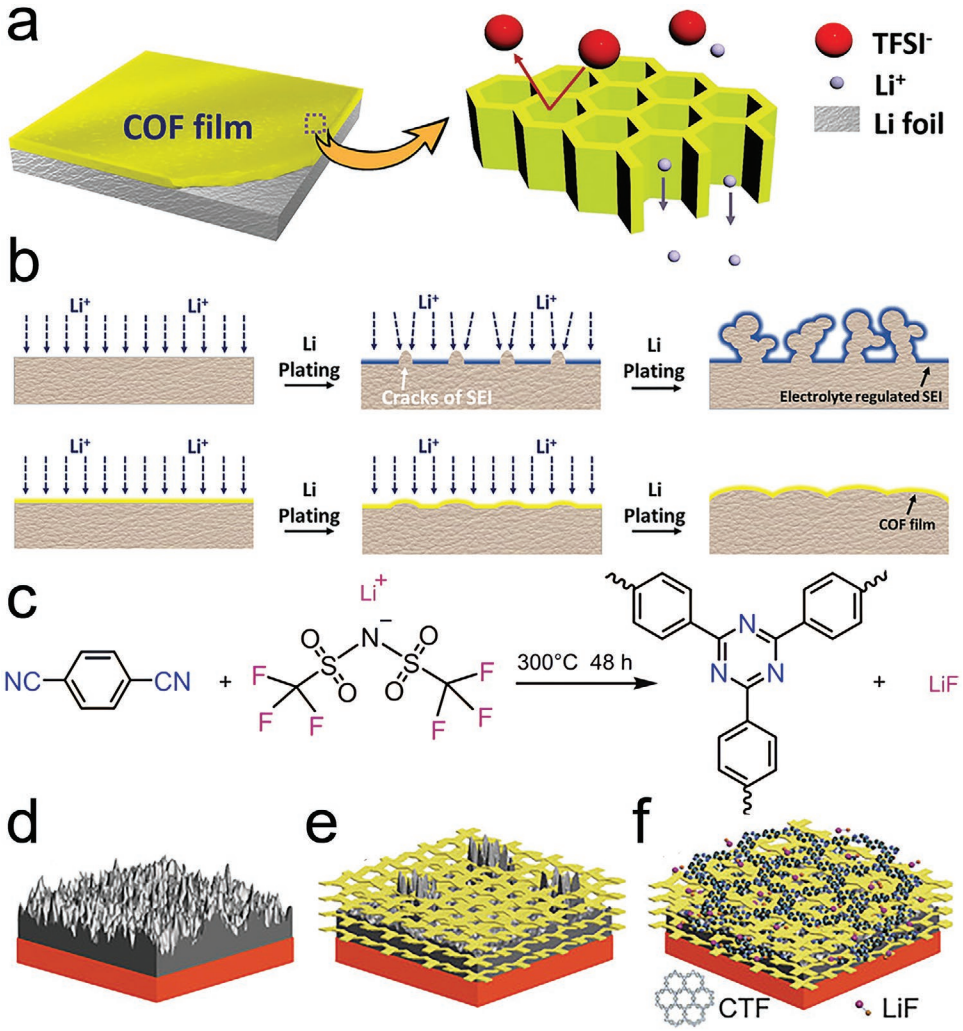

Figure 10. a) In situ preparation of TAPB-PDA COF on the surface of Li metal as an artificial SEI layer. b) Schematics showing the prevention of Li dendrite by COF SEI layer. a,b) Reproduced with permission.[92] Copyright 2020, Wiley-VCH. c) Diagrams for one-pot synthesis of CFT-1 with the presence of LiTFSI. Schematics showing Li dendrite growth situations on d) bare Cu, e) airlaid-paper (AP), and f) AP-CTF-LiF electrodes upon Li plating. c–f) Reproduced with permission.[94] Copyright 2019, Wiley-VCH.

Effective separators play a vital role in improving battery performance, including rate performance, cycle stability, safety, etc.[33–36,97] COFs are excellent potential separator materials due to their high stability, regular porosity, good mechanical property, and structural tunability.[98–102] The high stability of COFs help prevent their decomposition or reaction with electrolyte during the charge and discharge process.[6,8–10,98–102] High and uniform porosity enables the transport of ions, adequate retain of electrolyte, and uniform current density.[6,8–10,98–102] Excellent mechanical property prevents breakage during battery assembly and operations, while structural tunability ensures the wettability of electrolytes and efficient transport of Li^+.[6,8–10,98–102] Several publications have shed light on improving battery performance using COFs or COF composites as separators.[98–102] Applications of COFs or COF composites as separators in Li-S battery or Li-Se battery have successfully alleviated the shuttle effect and enhanced the cycling stability of batteries, which will be discussed in the Li-S battery section and other advanced battery section.[99–102] In LIBs, COFs were coated on a commercial polymer separator and successfully suppressed the penetration of transition metal ions and enhanced the Li^+ transportation simultaneously, thus improving the Li^+ transfer numbers.[98] Pure commercial polymer separator showed a limited Li^+ transfer number of 0.38, while COF coated commercial polymer separator displayed a high Li^+ transfer number of 0.76 in $[Li_{0.2}Mn_{0.55}Ni_{0.15}Co_{0.1}]O_2$/Li cell.

3. Li-S Batteries

Li-S batteries are also ideal candidates for next-generation energy storage devices due to the extremely high theoretical specific capacity of 1675 mAh g^{-1} and energy density of 2600 W h kg^{-1}.[103,104] They are composed of a lithium metal anode and sulfur cathode, and the natural abundance and low cost of sulfur make this type of battery highly attractive.[34,105–107] However, the use of Li-S batteries is constrained due to stability issues related to the "shuttle effect."[105–107] The

"shuttle effect" refers to the formation of soluble polysulfides during the charge-discharge process that can pass through the membrane separator, react with the lithium anode, and generate insoluble Li_2S and Li_2S_2.[105–108] "Shuttle effect" causes the loss of cathode sulfur and decreases the cycle stability.[105–108]

To overcome the shuttle effect of Li-S batteries, a variety of porous host materials have been used to physically entrap sulfur and thus reduce the unexpected transport of polysulfides during cycling.[108,109] In these studies, the host material often acts as cathode, and sulfur is impregnated into the host material through melt diffusion.[110] Host materials with high surface areas, such as CNTs,[111] graphene oxide,[112] MOFs,[113] porous carbons,[114] and conducting polymers,[115,116] have been extensively investigated. While physical confinement of polysulfides using these materials has proved to enormously enhance the recycling stability, shuttling still occurs due to the weak chemical confinement of polysulfides in the pores. Alternatively, other researchers employed chemical entrapment techniques to bind sulfur onto polymers through a copolymerization technique. For example, Pyun and coworkers introduced an "inverse vulcanization" approach where sulfur radically copolymerized with arylethenyl monomers.[117] Chemical entrapment improves the sulfur loading and enhances the sulfur-polymer interaction. However, problems such as detachment of sulfur during cycling loading and high insulation of copolymers still exist and prevent the excellent performance of Li-S batteries. Other chemical confinement techniques include N- or B-dopings.[118] N-doping can trap polysulfides through N-Li^+ interaction,[119] while B-doping enhances the interaction between the host materials with positively polarized boron and polysulfide anions. However, low doping ratios and low surface areas of the host materials limit the confinement efficiency.

COFs are promising host materials for Li-S batteries because researchers can optimize the physical and chemical confinement of polysulfides simultaneously through tuning the pore size and geometry and incorporating chemical functionalities.[9,120,121] Here, we review COFs as host materials of the cathode in Li-S batteries and further discuss methods of impregnating the material with sulfur, including physical tuning for improved sulfur loading and cyclability and chemical tuning for improved performance. Finally, we briefly discuss COFs as separators in Li-S batteries. The electrochemical performance of COF-related Li-S batteries is summarized in **Table 4**.

Table 4. Summary of Li-S batteries.

COF Name	Initial capacity	Cycling capacity	Current rate	Pore size [nm]	Sulfur loading	Method	Year	Ref.
Triazine–CTF-1	1197	762 @ 50 cycles @ 150 C	0.1 C	1.23	34%	Melt-diffusion	2014	[19]
Azo-COF	1536	741 @ 100 cyccles	0.1 C	2.6	0.6–0.8 mg cm^{-2}	Melt-diffusion	2015	[128]
COF-CNT-net				1.5/2.7	N/A	N/A (separator)	2016	[134]
Triazine–CTF-1	482	413 @ 300 Cycles	1 C	1.23	62%	In situ	2016	[136]
Boronate ester	1628	929 @ 100 cycles	0.2 C		40%	Melt-diffusion	2016	[126]
Porphyrin	1166	633 @ 200 cycles	0.5 C	1.55	55%	Melt-diffusion	2016	[127]
Fluorinated triazine	≈1100	833 @ 150 cycles	0.5 C		51%	In situ	2017	[21]
Fluorinated triazine	1138	928 @ 300 cycles	0.05 C		86%	In situ	2017	[123]
DMTA-COF	1415	1000 # 100 cycles	0.5 C	0.56	N/A	N/A (separator)	2018	[100]
Triazine + boroxine	808	663 @ 800 cycles	1 C	1.2	40–58%	Melt-diffusion	2018	[137]
Pyrene	1064	963 @ 100 cycles	1 C		70%	Melt-diffusion	2018	[122]
TP-PA-CNT	951	525 @ 450 cycles	0.5 C	1.3	N/A	CNT-templated	2018	[129]
Porphyrin	955	773 @ 200 cycles	0.5 C	1–10	1.1 mg cm^{-2}	Templated hollow-sphere	2018	[125]
Nitrogen doped graphitic carbon	869	670 @ 200 cycles	1 C	≈1.3	67.50%	Melt-diffusion	2018	[130]
Fluorinated	1120	645 @ 100 cycles	0.1 C	2.8	60%	Melt-diffusion	2018	[124]
Boron/oxygen doped COFs on CNTs	1210	794 @ 500 cycles	1 C	3.2	68.50%	Melt-diffusion	2018	[138]
Imine TAPB-PDA	1357	710 @ 200 cycles	0.2 A g^{-1}	3	60%	Melt-diffusion	2019	[139]
Redox-active keto/pyridine units	1184	977 @ 100 cycles	0.2 C	2.2	N/A	N/A (separator)	2019	[101]
Fluorinated	1287	904 @ 1000 cycles	0.5 C	1.18	70%	Melt-diffusion	2019	[20]
Lithiated COF nanosheets	982	≈620 @600 cycles	1 C	1.4	N/A	N/A (separator)	2020	[135]
COF-CNT nanocomposite	1047	568 @ 700 cycles	2 A g^{-1}	2–8	N/A	N/A (separator)	2020	[140]
Triazine/polypyrrole channels	699	682 @ 500 cycles	1 C		83%	In situ	2020	[141]
COF-CNT nanosheets	1030	798 @ 50 cycles	0.2 C	1.25/2.7 nm	78%	CNT templated/ melt-diffusion	2020	[142]

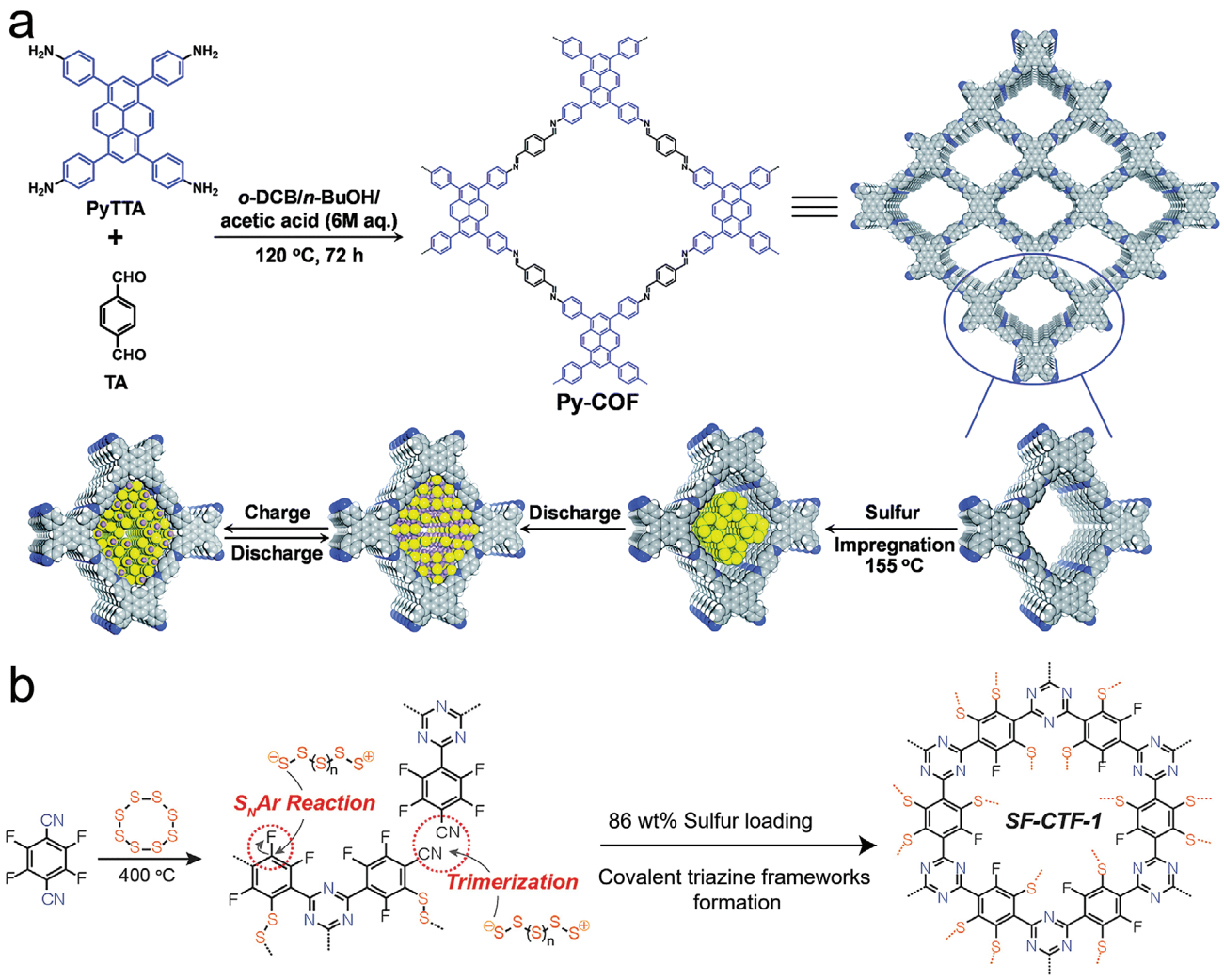

Figure 11. a) Py-COF and Py-COF/S composites. Reproduced with permission.[122] Copyright 2018, Royal Society of Chemistry. b) CTF-1/S@155 °C composite. Reproduced with permission.[123] Copyright 2017, Wiley-VCH.

3.1. COFs for Sulfur Cathode Hosts

Sulfur loading, or content, within the host material in Li-S batteries is the most significant factor that impacts their capacity, cyclability, and rate performance. High sulfur loading is more ideal for better electrochemical performance. Currently, two impregnation methods to load sulfur are mainly studied. One is melt diffusion, where COF and sulfur are heated, and molten sulfur penetrates the COF matrix. The other is in situ impregnation, where sulfur is anchored onto COFs through covalent bonds during the polymerization process. Melt diffusion does not depend on the COF chemistry and structure and shows a broader application scope, but the sulfur loading amount is relatively low. Sulfur loading has now improved from 34%[19] to 70%[122] (see **Figure 11**a, sulfur loading in Py-COF) through tuning the chemical structures of COFs. In situ impregnation produces higher sulfur loading up to 86%, as reported by Coskun and coworkers[123] (Figure 11b), and offers a simple, one-pot synthesis method. However, it only applies to a limited scope of COF chemistries that can interact with sulfur through chemical reactions.

Tuning the physical structure, such as pore size, crystallinity, and the preparation of hollow structures, has also proved effective for sulfur loading. Researchers have found that larger pore sizes (>2 nm) enable higher sulfur loading, faster lithium transport, and improved cyclability compared to smaller pore sizes (≈1.2 nm).[19,122] In a study of fluoro-substituted COFs (**Figure 12**a), Wang and coworkers illustrated that improved crystallinity of the COF leads to higher sulfur loading, higher electrochemical activity, faster kinetics due to efficient ion-diffusion, and enhanced electrical conductivity caused by the improved stacking of 2D sheets.[124] However, crystalline COFs showed poorer cyclability than their amorphous counterparts, which possibly resulted from the easier polysulfide migration along the 1D channel in crystalline COFs. Recently, Zhang and coworkers demonstrated that hollow COF spheres (Figure 12b) improved the cycling life of Li-S battery.[125] Hollow structures were prepared through in situ COF polymerization

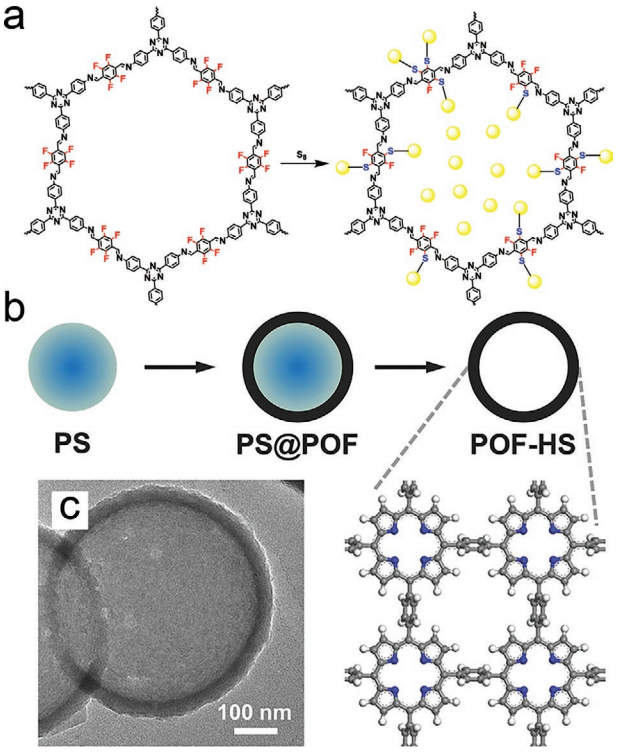

Figure 12. Schematic for the synthesis of a) COF-S composite and b) hollow COF spheres. a) Reproduced with permission.[124] Copyright 2018, American Chemical Society. b) Reproduced with permission.[125] Copyright 2017, Wiley-VCH.

with polystyrene (PS) microsphere as templates and sequential removal of PS templates (see Figure 12b). The hollow sphere design is desirable and has been studied for many different applications due to its low density, large surface area, and improved structural integrity. For Li-S batteries, hollow spheres are advantageous because sulfur can be trapped inside the spheres, and the hollow structure can tolerate the volumetric changes during cyclings. The reported COF hollow sphere host material demonstrated good performance and cyclability with Coulombic efficiency near 100% after 200 cycles.

Chemical tunings of COF structures and chemistries also exhibit a broad application scope and lead to much higher sulfur loading than physical tunings. A triazine COF (CTF-1, see structure in Figure 11b) was first reported by Wang and coworkers[19] in 2014 to have been used in Li-S batteries. CTF-1 showed high privilege in applications of Li-S batteries due to its high thermal stability and narrow pore size distributions. However, only a low loading of sulfur (34 wt%) was produced through melt diffusion. Furthermore, no chemical interactions of sulfur with COFs make the sulfur easy to lose. Consequently, the battery only showed good cyclability at elevated temperatures because sulfur diffused out of the COF matrix very easily at room temperatures. To address these issues, Coskun and coworkers developed an in situ sulfur impregnation method to load sulfur in CTF-1 through a stepwise approach.[123] Elemental sulfur first underwent ring-opening polymerization and turned into linear polysulfane at 160 °C. Then, the singlet state of sulfur in linear polysulfane further underwent C—H insertion reactions and impregnated with CTF-1 through covalent bonds simultaneously. The sulfur loading was increased to 62% by using this method and showed good cyclability (84.3% capacity retention after 50 cycles at 0.2 C) at room temperature.

Fluorination of COFs is also widely investigated as an effective approach for chemical tuning of sulfur (Figures 11b, 12a). Coskun and coworkers[123] designed a fluorinated CTF-1 and formed a SF-CTF-1 composite through a nucleophilic aromatic substitution reaction between the fluorinated units and the elemental sulfur (see Figure 11b). This increased the number of sulfur chains (from one to four) that were attached to each linkage group within the COF compared to the original CTF-1 reported by Zhang and coworkers.[19] As a result, the sulfur loading increased to 86%, and the cycling performance of the battery improved compared to its non-fluorinated counterpart.

Boronate ester functionality also proves as an effective moiety for chemical confinement of sulfur in COFs and improvement of cycling stability of Li-S batteries. Tang and coworkers[126] reported that COFs with boronate ester linkages exhibited improved chemisorption of polysulfide compared to triazine COFs. Positively polarized B within the pores enhanced the absorption of S_x^{2-} and the negatively polarized O units adsorbed Li^+ more effectively and trapped lithium polysulfides more efficiently than triazine COFs. Thus, boronate ester COF showed better cycling stability than the triazine COF (boronate ester COF: discharge capacity of 929 $mAhg^{-1}$; triazine COF: 489 $mAhg^{-}1$ after 100 cycles at 0.2 C). Density functional theory (DFT) simulations further confirmed that COFs with boronate ester linkages had a lower S_x^{2-} adsorption energy and better anchoring of Li_2S_x to the pores compared to triazine COFs (see **Figure 13**).

Other COF chemistries, including porphyrin,[127] azo,[128] and pyrene COFs[122] were also extensively investigated as host materials for Li-S cathodes since they shared large pore sizes and enabled high sulfur loadings. Additionally, the incorporation of COF and multi-wall CNTs were also studied by Wei and coworkers to enhance the electrical conductivity of host materials.[129] The resulting cathode offered an initial discharge capacity of 1242 mAh g^{-1} at 0.05 C and an ultra-low capacity fade rate of 0.099% per cycle. Nitrogen-doped graphitic carbon through the carbonization of a COF was also reported to have increased the electrical conductivity and sorption properties of the host material before sulfur was melt-diffused into the pores.[130] This resulted in a battery with an initial discharge capacity of 1598 mAh g^{-1} at 0.03 C and nearly 100% Coulombic efficiency during the cycling test.

3.2. COFs-Based Separators

COF-based host materials cannot completely suppress the dissolution of lithium polysulfides from the sulfur cathode, so the specific capacity of Li-S batteries still decreases during charge-discharge cycles.[104,116] Functional separators with surface coatings can further reduce the diffusion of lithium polysulfides. Coating materials on separators can chemically adsorb the escaped lithium polysulfides,[131] catalyze sulfur reduction,[132] and enhance the heat transfer inside Li-S batteries.[133] Furthermore, the coating materials can prevent the blocking of

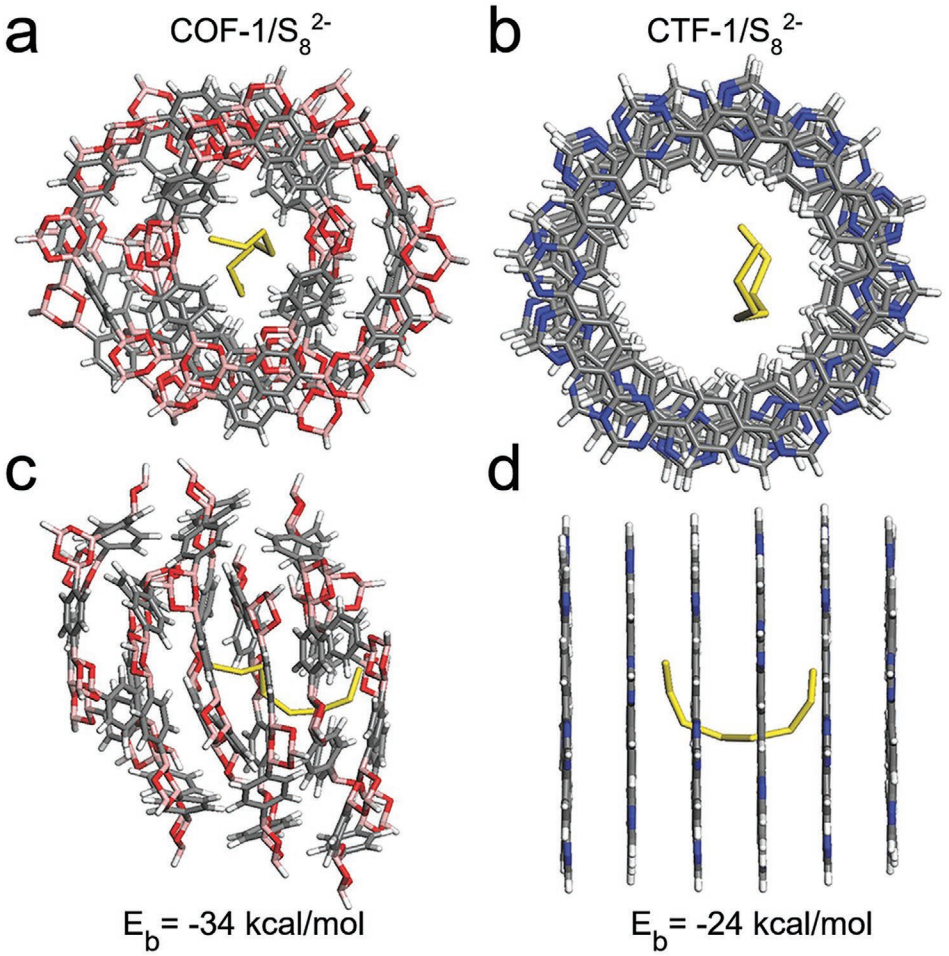

Figure 13. Quantum mechanics/molecular mechanics-calculated adsorption energy for S_8^{2-} anions in pores of COF.[126] Reproduced with permission.[126] Copyright 2016, Wiley-VCH.

open pores by solid electrolytes and the impaling of separators by the lithium dendrite; thus, they enhanced the safety for Li-S batteries[131] during cycling at high current densities.

In 2016, Lee and coworkers reported a hierarchical porous separator with chemical trap functions comprised of a COF-net on a CNT-net.[134] The mesoporous structures of the CNT-net enabled fast ion transport through the separator, and the microporous structures of the COF-net effectively alleviate the "shuttle effect." Coating of lithiated COF nanosheets/graphene on commercial Celgard separators also proved effective for improved Li^+ transport and efficient blocking of polysulfides simultaneously compared to pure graphene coating.[135] Triazole groups in the COF nanosheets could coordinate with polysulfides through the N-Li bond and effectively blocked the diffusion of polysulfides. Therefore, the as-prepared Li-S batteries exhibited a high initial capacity (982 mAh g^{-1} at 1 C) and a low capacity decay (0.057% per cycle after 600 cycles). Cai and coworkers[100] coated a ceramic separator using a COF with rhombic topology. The Li-S battery assembled with this separator realized an initial capacity of 1415 mAh g^{-1}, and it decayed slowly to 1000 mAh g^{-1} after 100 cycles at 0.5 C, which far outperformed the bare ceramic separator. Li and coworkers[101] also reported a redox-active pyridine-based COF separator. The pyridine units as the redox-active group were able to catalyze the conversion of polysulfides and reduce the "shuttle effect." Therefore, the battery exhibited a specific capacity of 977 mAh g^{-1} at 0.2 C after 100 cycles, which was 5.2 times higher than that of the Li-S battery without a COF separator.

To summarize, COFs are very promising materials to help achieve the theoretical capacities and energy densities of Li-S batteries by catalyzing the conversion of polysulfides and reducing the shuttle effect of polysulfides. Researchers have shown that physical tuning, including control of pore size, crystallinity, and hollow structures, could impact sulfur loading, and chemical tuning like fluorination of pores and introduction of boronate ester moieties can increase the sulfur loading and improve cyclability of Li-S battery. Additionally, COFs are promising as separators in Li-S batteries and can significantly improve cycling performance. However, the electrical conductivity of COF-based hosts needs further improvement; thus, the sulfur content and loading could be enlarged, and the energy density of Li-S batteries could be increased. The effect of functional COF separators on inhibiting lithium dendrites in Li-S batteries also remains to be thoroughly studied in the future.

4. Applications of COFs in SIBs/PIBs

The rapid development of LIBs and the large excess of lithium utilization have brought concerns about insufficient supplies of lithium resources.[42,143,144] So, it is necessary to develop new energy storage technology to resolve the lithium shortage problems and satisfy future market needs. SIBs and PIBs have gained considerable attention due to their abundant resources and lower cost.[5,42,143,145–149] In addition, Na and K are located below Li in the periodic table and share similar intercalation chemistry as Li, and the intercalation mechanism has been well established.[5,42,143,145–149] SIBs currently face the challenges of low energy density and poor cycling stability, which limits their commercialization.[5,42,145,146] Exploration of novel electrode materials is essential to improve energy density and enhance cycling stability. The poor electrochemical performance of SIBs originates from the lower ionization potential of Na^+ (the standard electrode potential versus SHE of Na^+/Na is −2.714 V, and the practical reduction potential of Na^+/Na in organic solvents is ≈2.56 V), which is much lower than Li^+/Li (the standard electrode potential versus SHE of Li^+/Li is −3.040 V, and the practical reduction potential of Na^+/Na in organic solvents is ≈2.79 V).[5,42,145,146] As a result, SIBs have a lower operating voltage window and low energy density. Additionally, Na-intercalation did not function as well as Li-intercalation due to the larger size of Na^+ radius and severe volume expansion of electrode, leading to the loss of electric contact and fast capacity fading.[5,42,145,146] Researchers have explored to use COFs as electrode materials to overcome those drawbacks and improve their electrochemical properties. Organic COFs with 2D layered structures are more flexible in mechanical property compared to inorganic materials, and thus they experience a relatively lower volume expansion during the Na-intercalation.[150] As for PIBs, the reduction potential of potassium (≈2.936 V versus SHE and the practical reduction potential of Na^+/Na in organic solvents is ≈2.88 V) is between Na and Li, so it has a relatively higher energy density.[143] Furthermore, much weaker Lewis acidity of K causes smaller solvated ions, which resulted in improved conductivity and increased ion transfer amounts compared to Na and Li.[148,151] Lower desolvation energy of K^+ could also promote the faster diffusion of K^+ through the electrolyte/electrode interface.[148] However, the large size of K^+ radius makes it challenging to select electrode materials. Several recent studies have investigated COFs in PIBs and realized excellent electrochemical performance,[51,65,152] paving ways for COFs as promising electrode materials in this area.

4.1. COFs in SIBs

Researchers have explored the applications of COFs as electrode materials in SIBs and focused on elucidating their structure-performance relationship and understanding the Na-intercalation mechanism. For example, Pradhan and coworkers[150] found that conjugated structures and triazine functionalities were advantageous for intramolecular electron transfer, making the conjugated COFs containing triazine moieties very promising in SIBs. A SIB half cell with triazine COFs as anode exhibited an average capacity of 245, 200, 170, and 145 mAh g^{-1} at current densities of 30, 50, 100, and 200 mA g^{-1}. However, an irreversible SEI layer formed in the first cycles, consumed enormous Na^+ and led to a very low Coulombic efficiency. Park and coworkers uncovered the relationship between surface areas of COFs and electrochemical properties.[153] They found that COFs with higher surface areas demonstrated a higher Na^+ storage ability compared to the COFs with identical backbones and lower surface areas. They also discovered that enforcement of backbone structures could improve the charge-carrier conductivity and further enhance the Na^+ storage capability. Vaidhyanathan and coworkers unraveled the relationship between molecular-level electronic structure and SIB performance.[154] The band gaps of COFs were tuned through the introduction of heteroatom N in the COF structures. They found that COFs with lower lowest unoccupied molecular orbital (LUMO) levels enabled easier electron accumulations and outperformed other COFs with higher LUMO levels. Furthermore, Chen and coworkers found that a nitrogen-rich COF (TQB-COF, see **Figure 14**a) achieved a very high reversible capacity of 452.0 mAh g^{-1} and retained 352.3 mAh g^{-1} after 100 cycles at 0.02 A g^{-1}.[155] This COF had an extremely high content of nitrogen (23.8 wt%), and the introduction of N atoms decreased the bandgap and thus led to improved electronic conductivity (≈10^{-9} S cm^{-1}) and enhanced ionic conductivity (≈10^{-4} S cm^{-1}). TQBQ-COF also exhibited prominent rate capability (134.3 mAh g^{-1} at 10.0 A g^{-1}) and superb cycling stability with a capacity retention of 96% even after 1000 cycles at 1.0 A g^{-1}.

Exploration of the Na storage mechanism is also necessary to understand the working discipline of SIBs. Unlike LIBs, which have a well-understood Li storage mechanism, the Na storage mechanism is relatively ambiguous and remains to be elucidated. For example, Chen and coworkers proposed a "12 Na^+ insertions and extractions" mechanism of TQBQ-COF[155] (see Figure 14a). To study the mechanism, they employed in situ/ex situ Fourier-transform infrared spectroscopy (FTIR) and ex situ X-ray photoelectron spectroscopy to observe the changes of C=O and C=N functionalities during the charge-discharge process. DFT calculations were also used to understand the possible structure changes during the electrochemical process (see Figure 14b). TQBQ-COF had a hexagonal topology with a pore size of 1.14 nm. The molecular electrostatic potential (MESP) method predicted that six equivalent minima of electrostatic potential corresponding to six Na^+ could be accommodated in the middle of two adjacent nitrogen atoms within the molecular plane. Furthermore, the MESP method confirmed that no Na^+ could be accommodated in the ring units, and another six Na^+ could be accommodated between two adjacent oxygen and nitrogen atoms outside of TQBQ-COF plane (Figure 14b). In another report by Lu and coworkers, they studied the sodium storage mechanism through ex situ electron paramagnetic resonance analysis.[156] They found that radical intermediates C–O· and α-C existed and interacted with Na^+ in a total of four different steps (see Figure 14c). For the discharge process, one carbonyl moiety in the anthraquinone unit would react with sodium ions, and the other would transform into C–O· radical (Structure B). Carbonyl groups of the anthraquinone unit in structure B further reacted with another sodium ion and formed structure C containing sodium alcoholate units. Afterward, the carbonyl groups of β-keto units coordinated with Na^+

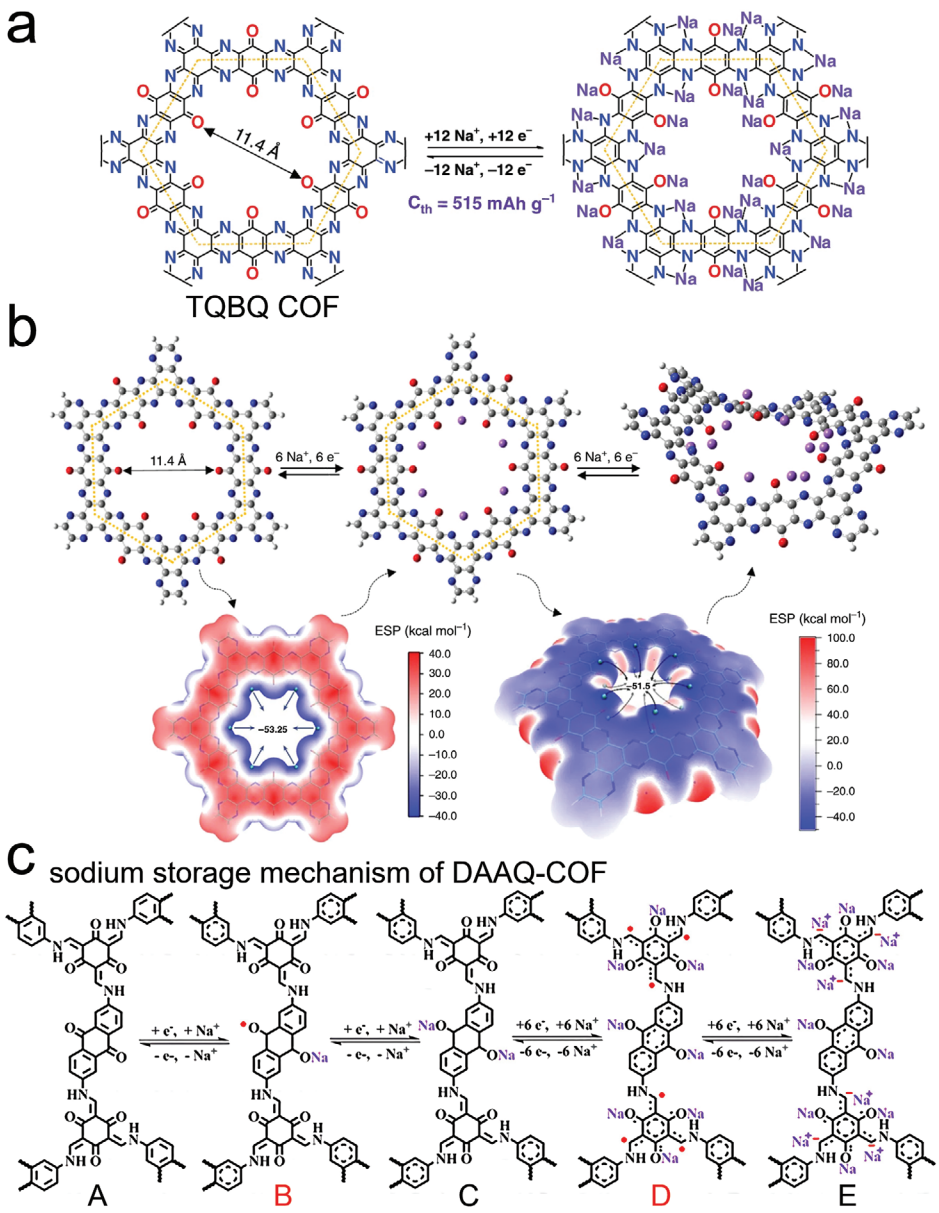

Figure 14. a) TQBQ-COF structure and schematics of 12 e^- storage mechanism b) Schematic diagram of the two-step sodiation and desodiation process of the TQBQ-COF calculated through the MESP method. a,b) Reproduced with permission.[155] Copyright 2020, Nature Publishing Group. c) Sodium-ion storage mechanism of DAAQ-COF. Reproduced with permission.[156] Copyright 2019, American Chemical Society.

and formed structure D containing α-C radicals. α-C radicals were electrophilic and could accept more electrons to form α-C anion, which further coordinated with Na^+ to form structure E. The charging process took a reverse procedure compared to the discharging process.

4.2. COFs in PIBs

Current studies on applications of COFs in PIBs mainly focused on designing optimal COF structures to realize better battery performance. For example, a few-layer boronic ester-based COF (COF-10) and CNT composite (**Figure 15**a,b) were used as anode in PIBs for the first time reported by Wang and coworkers.[65] They discovered that π-conjugated structures could generate strong π-K^+ interactions and serve as a promising electrode for PIBs. Exfoliated COF nanosheets exposed more active sites, and the incorporation of CNTs enhanced electron transport, so few-layer COF-10@CNT anode demonstrated very large capacities (288 mAh g^{-1}) even after 500 cycles at the current density of 0.1 A g^{-1}. More impressive, it showed a capacity of 161 mAh g^{-1} after 4000 cycles at a high current density of 1A g^{-1} (Figure 15c). Fluorination of pore channels and few-layer structures of COFs are also effective approaches

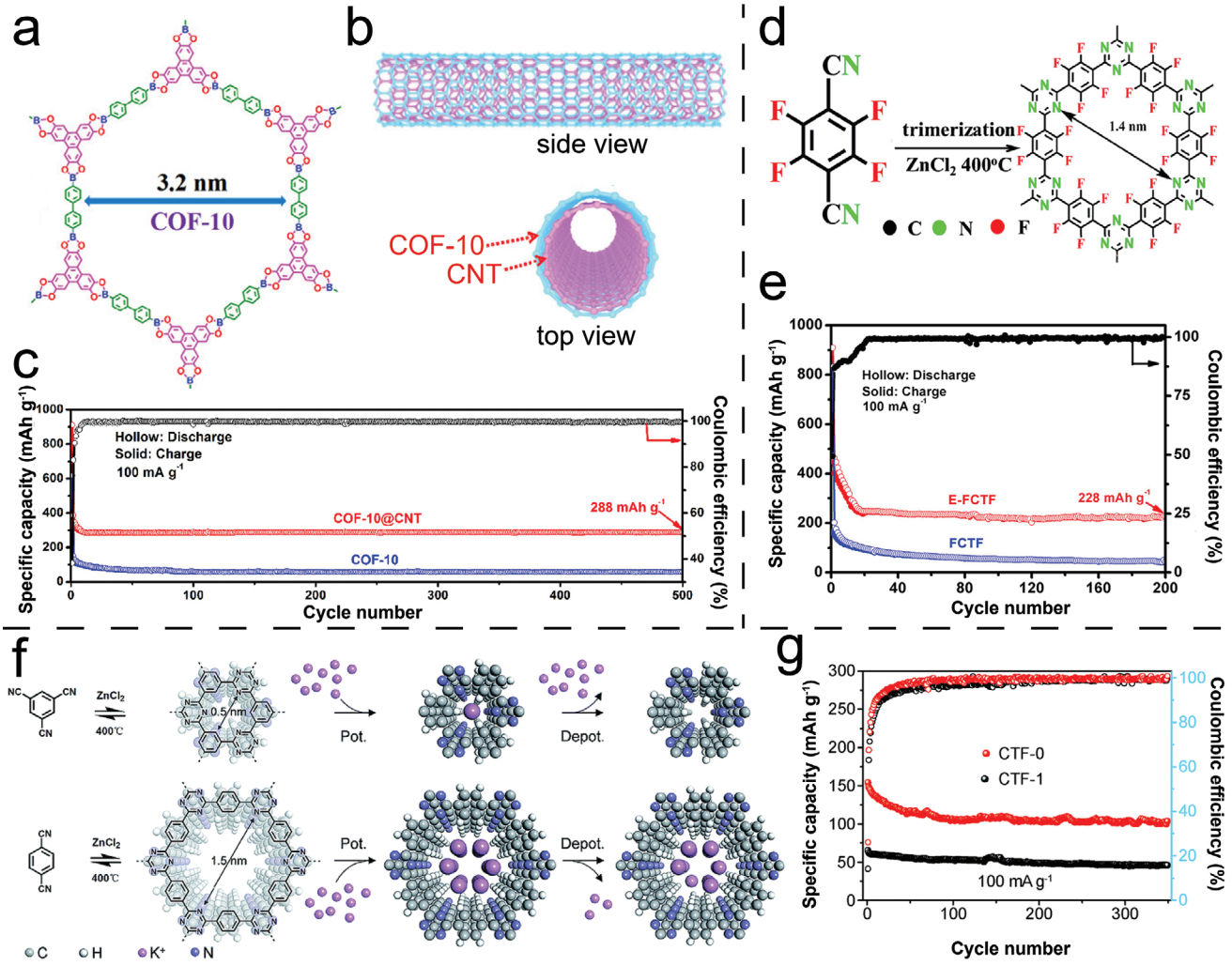

Figure 15. a) Chemical structures of boronic ester-based COF (COF-10). b) Side view and top view of COF on the surface of CNT. c) Cycling performance of COF-10@CNT. a–c) Reproduced with permission.[65] Copyright 2019, American Chemical Society. d) Synthesis of bulk FCTF via the trimerization of tetrafluoroterephthalonitrile catalyzed by $ZnCl_2$. e) Cycling performance of exfoliated FCTF COF (or E-FCTF) and FCTF at 0.1 A g^{-1} for PIBs. d,e) Reproduced with permission.[51] Copyright 2019, American Chemical Society. f) Schematics for the synthesis of CTFs and the corresponding potassiation/depotassiation process in CTFs with different pore sizes (CTF-0 and CTF-1). g) cycling performance of CTF-0 and CTF-1. f,g) Reproduced with permission.[152] Copyright 2019, Royal Society of Chemistry.

to improve the electrochemical performance in PIBs. Wang and coworkers further designed a few-layer fluorinated triazine CONs (E-FCTF, Figure 15d) by trimerization in molten $ZnCl_2$ followed by micromechanical exfoliation and employed the CONs in PIBs[51] (Figure 15e). The presence of fluorine atoms narrowed the bandgap of CTF and increased the electron transfer capability. Few-layer structures reduced the alkaline transport distance and resolved the sluggish diffusion problems. The exfoliated E-FCTF anode exhibited excellent cycling performance and retained a high capacity of 228 mAh g^{-1} after 200 cycles. Pore size is also one crucial factor that impacts the electrochemical performance of PIBs. Zhu and coworkers[152] recently studied the pore size effects on the CTF anode by comparing the electrochemical behavior and molecular mechanistic simulations of CTF-0 (with pore size ≈0.5 nm) and CTF-1 (with pore size ≈1.5 nm) in PIBs (Figure 15f,g). They found CTF-0 with a smaller pore size demonstrated better electrochemical performance than CTF-1 with larger pore size. Tested at the current density of 100 mA g^{-1}, CTF-0 displayed a high capacity ranging from 154 to 113 mAh g^{-1} after 200 cycles, while CTF-1 had a 1ow capacity around 60 mAh g^{-1} (Figure 15f). Additionally, CTF-0 showed a better rate capacity and a better Coulombic efficiency than CTF-1 in the several initial cycles. Molecular mechanistic simulations revealed that deintercalation of K^+ from CTF-0 is exothermic, while the deintercalation of K^+ from CTF-1 is endothermic. The exothermic process is preferred, and thus CTF-0 showed a higher reversible capacity than CTF-1.

Currently, the application of COFs in SIBs/PIBs is limited to just a handful of COF structures. Rational design of optimal structures (e.g., carbonyl and radical functionalities) that can effectively interact with sodium and potassium ions is necessary. To understand the sodium/potassium intercalation

mechanism, in situ techniques should be adopted. For example, in situ FTIR is helpful in elucidating the structural changes during the charge-discharge procedures. Theoretical mechanistic analysis is also beneficial for the understanding of the structure-property relationship and further provides feedback on the structure design.

5. Applications of COFs in Li-CO_2 Batteries

Li-CO_2 battery is a new type of energy storage device that can directly utilize CO_2 gas and transform it into energy.[157–160] Appropriate CO_2 cathodes are vital components and demonstrate good CO_2 capture ability, low overpotential, high reversibility, and excellent rate performance.[159,160] COFs have abundant pores and demonstrate high CO_2 adsorption ability, especially for those COFs with an appropriate pore size that can effectively entrap CO_2 molecules. The most widely investigated imine COFs show better CO_2 adsorption ability since the basic nature of imine bonds can effectively interact with acidic CO_2 molecules. Additionally, COFs can be designed with CO_2-affiliative functionalities like amine groups in the pore channels, and they can also be incorporated with inorganic nanoparticles such as Ru nanoparticles to serve as a catalyst during the charge/discharge process.

By using COF/graphene composites (graphene@COF) as cathode, Meng and coworkers successfully reduced the shuttle effects of CO_2 (see schematics in **Figure 16**a) and improved the electrochemical performance of the Li-CO_2 battery (Figure 16b).[159] Pure graphene or pure COF only displayed a low CO_2 uptake ability, while graphene@COF demonstrated superb CO_2 uptake ability. A possible reason for

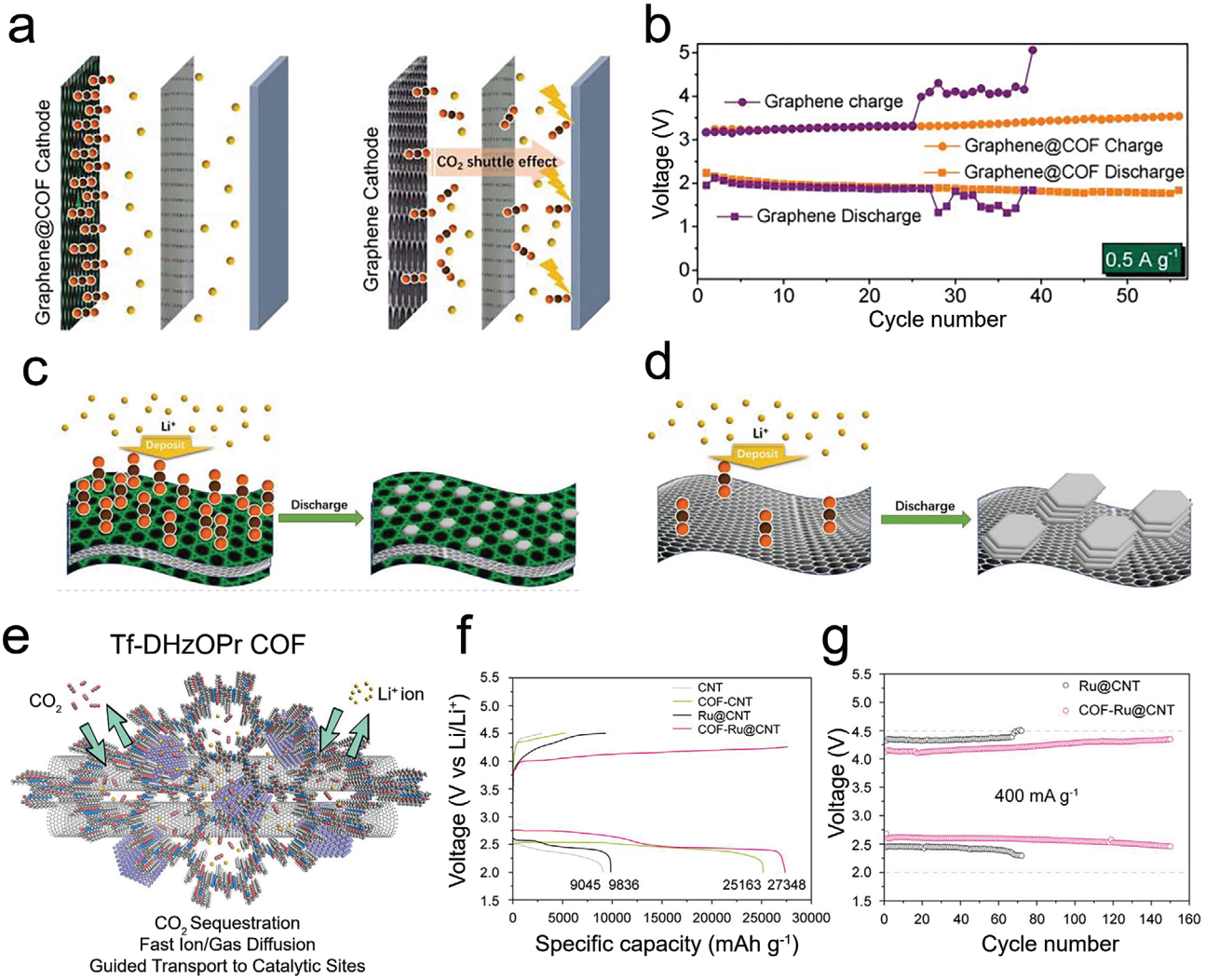

Figure 16. a) Schematics show that graphene@COF cathode helps reduce CO_2 shuttle effect compared to pure graphene cathode. b) Long-term cycling performance of the graphene battery and graphene@COF battery at the current of 0.5 A g^{-1}. c) Schematic for formation of small-size Li_2CO_3 reacted by depositing Li^+ on the cathode and the nanoenriched and nanoconfined CO_2. d) Schematic for formation of large-size Li_2CO_3 reacted by deposited Li^+ on the cathode and the loose CO_2. a–d) Reproduced with permission.[159] Copyright 2019, Wiley-VCH. e) Schematics for Tf–DHzOPr COF incorporated with Ru@CNT. f) Full discharge curves of different cathodes at a current density of 200 mA g^{-1}. g) Life cycles of Ru@CNT cathode and COF-Ru@CNT cathode at 1000 mA g^{-1}. e–g) Reproduced with permission.[160] Copyright 2019, Wiley-VCH.

the improved CO_2 adsorption was related to the higher density of exposed micropores of COFs induced by the graphene templated growth process. Without graphene, only nonporous amorphous structures could be produced at that reaction conditions (25 °C, 5 h). The composite effectively enriched and confined CO_2 without decreasing the electron conductivity of graphene. The overpotential of graphene@COF battery only increased gradually from 1.08 to 1.70 V after 56 cycles under a high rate of 0.5 A g^{-1}, and the charge voltage reached just 3.54 V. However, graphene battery only showed reversible capacities before the 26th cycle and achieved a very high overpotential (3.23 V) and charge voltage (5.06 V) at 39th cycle (Figure 16b). The stability of the Li-CO_2 battery is highly correlated to the consumption of Li^+. On graphene@COF, small-size Li_2CO_3 particles formed within the micropores during the discharge process and decomposed into Li^+ and CO_2 in the charge process (Figure 16c), indicating a reversible Li consumption and regeneration. However, large-size Li_2CO_3 particles formed on pure graphene cathode randomly in the discharge process and did not fully decompose in the charge process (Figure 16d), so increasing amounts of Li were consumed after cycles.

Loh and coworkers[160] also reported a COF-based Li-CO_2 battery by incorporating hydrazone COFs with Ru nanoparticle-decorated CNTs (Ru@CNT) as illustrated in Figure 16e–g. Hydrazone COFs served as effective CO_2 collectors during the charge/discharge process to improve the energy capacity, and they also acted as the diffusion layers for both Li^+ and CO_2 molecules to improve the rate performance. Ru nanoparticles worked as catalysts and facilitated the kinetics during the charge/discharge process, and CNT promoted electron mobility. This COF-based cathode exhibited a low overpotential of 1.24 V, and the Li-CO_2 batteries displayed a capacity of 27 348 mAh g^{-1} at 200 mA g^{-1} (Figure 16f), which was much higher compared to the widely used Ru@CNT cathode (9836 mAh g^{-1} at 200 mA g^{-1}). In addition, the Li-CO_2 battery only possessed a low discharging voltage loss even at 4000 mA g^{-1} and demonstrated superior cycling stability (200 cycles at 1000 mA g^{-1}, Figure 16g). The excellent electrochemical performance was attributed to the synergistic effects of COF, Ru nanoparticles, and CNT. First, the hydrazone COF had a superb CO_2 uptake capacity (65.8 cm^3 g^{-1} (1 atm, 248 K), 51.2 cm^3 g^{-1} (1 atm, 273 K), and 25.6 cm^3 g^{-1} (1 atm, 298 K)) and had ordered 1D channels that enabled the fast Li^+ mobility. Second, Ru nanoparticles served as an effective catalyst for CO_2 reduction and $LiCO_3$/C decomposition. Third, the incorporation of CNT promoted the electron transfer of the COF-based electrode and reduced the internal resistance.

6. Application of COFs in Zinc-Ion/Air Batteries

6.1. ZIBs

ZIBs are also promising alternatives for LIBs due to the desired properties of zinc anode, such as high capacity density (5855 mAh cm^{-3}), low cost, abundant resources, good chemical/physical stability, and environmental friendliness.[161–163] Similar to LIBs, ZIBs are also composed of anode, cathode, electrolyte, and separator. Stable zinc metals are typically employed as an anode, which is safe and easy to fabricate.[161–163] The cathode is usually composed of layered materials serving as insertion hosts for Zn^{2+}.[161–163] Almost neutral or slightly acidic electrolyte (e.g., $ZnSO_4$ solution) is usually implemented and shows high stability.[161–163] A separator is also necessary to divide the anode and cathode in case of a short circuit.[161–163] Zinc ions move between the cathode and anode during the charging and discharging processes. Among these various components, the cathode materials are most widely investigated due to their crucial role. COFs can be rationally designed with abundant functionalities to serve as nucleophilic centers that interact with Zn^{2+}. For example, N=O and N−H functionalities are excellent nucleophilic centers that can coordinate with Zn^{2+}. Both N=O···Zn and Zn···N-H interactions are reversible and show promising applications in ZIBs. Porous structures also make it easier for Zn^{2+} to reach the nucleophilic centers.[164,165]

Banerjee and coworkers[164] reported a hydroquinone-linked β-ketoenamine COF (HqTp-COF, see **Figure 17**a) acting as a zinc-ion anchor in an aqueous rechargeable ZIB. Abundant C=O and N−H functionalities in the structures coordinated with Zn^{2+} reversibly during the electrochemical redox process, and thus HqTp-COF (Figure 17a) exhibited excellent electrochemical performance in ZIBs. It delivered a discharge capacity of 276.0 mAh g^{-1} at 125 mA g^{-1}. Additionally, HqTp cathode (Figure 17a) displayed a specific capacity of 85.0 mAh g^{-1} under the current rate of 3750.0 mA g^{-1} and retained 95% of its initial capacity even after 1000 cycles. It also kept an excellent Coloumbic efficiency of 98% throughout the 1000 cycles without any decline (Figure 17b). Four 1.75 V HqTp-zinc ion cells were further assembled in a series connection and could directly charge a smartphone device (Figure 17c).

Very recently, Alshareef and coworkers[165] designed a phenanthroline COF (PA-COF, Figure 17d) and successfully employed it as an electrode in zinc-ion supercapatteries (ZISs) for the first time. Supercapatteries represent a type of electrochemical energy storage device that takes advantage of both capacitive and non-capacitive Faradaic charge storage mechanisms. Phenanthroline functional groups with abundant nitrogen in the COF structure served as the active zinc ion storage sites and enabled the prominent electrochemical performance of the ZISs. The aqueous ZIS was composed of PA-COF cathode, Zn anode, and 1.0 M $ZnSO_4$ electrolyte. The PA-COF electrode exhibited an extremely high capacity of 247 mAh g^{-1} at a current density of 0.1 A g^{-1}. It showed just 0.38% capacity decay per cycle during 10 000 cycle discharging and charging processes (Figure 17e), which was claimed as the best cycling performance ever reported for COF materials in ZIB or capacitors.

6.2. Zn-Air Battery

In addition to ZIBs, Zn-air batteries are another type of zinc-based batteries under vigorous investigations.[167–169] A typical Zn-air battery consists of a zinc anode, an oxygen-permeable cathode, and an alkaline electrolyte. Zn-air batteries typically have a low cost due to the use of readily accessible and recyclable zinc and atmospheric oxygen. They have a high theoretical specific energy of 1218 $Wh \cdot kg^{-1,}$ and a high volumetric

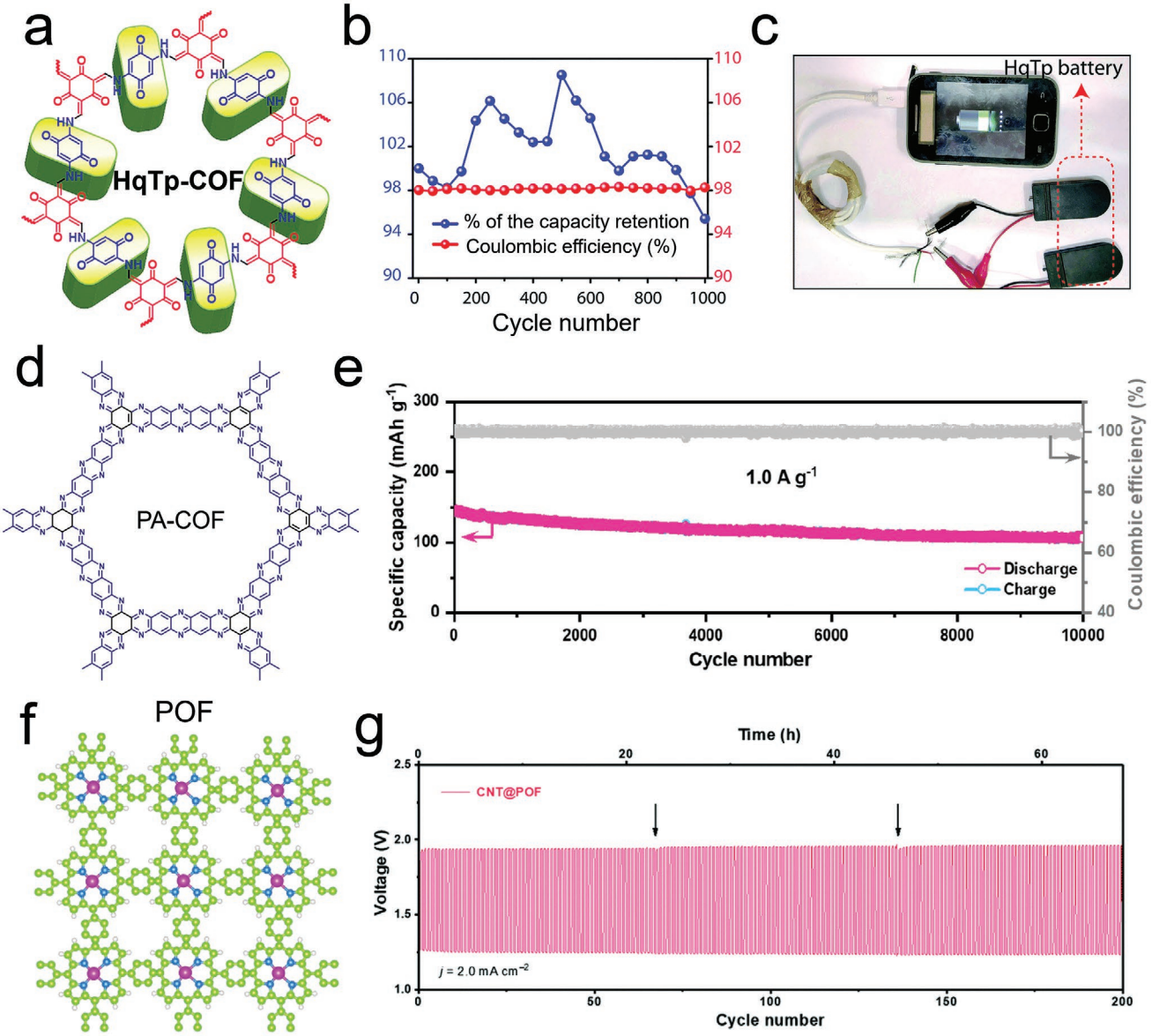

Figure 17. a) Structure of HqTp-COF (Hq: 2,5-diaminohydroquinone, Tp: 1,3,5-triformylphloroglucinol b) Long-life cyclic stability and Coulombic efficiency plot at 3750 mA g^{-1}. c) Digital photograph of charging a smartphone by Zn/HqTP cell. a–c) Reproduced with permission.[164] Copyright 2018, Royal Society of Chemistry. d) Structure of PA-COF, e) cycle performance of PA-COF. d,e) Reproduced with permission.[165] Copyright 2020, American Chemical Society. f) Chemical structure of POF. g) Long time cycling test of CNT@POF at 2.0 mA cm^{-2} (arrows represent replacement of the old electrolyte). f,g) Reproduced with permission.[166] Copyright 2018, Royal Society of Chemistry.

energy density of 6136 $Wh \cdot L^{-1}$.[170] They are considered safe as they rely on a non-flammable aqueous electrolyte. Although most Zn-air batteries are primary batteries, they can be recharged by replacing the zinc anode and the electrolyte mechanically; otherwise, they can also be regenerated by catalyzing the oxygen reduction reaction during the discharge process and the oxygen evolution reaction during the recharge process at the cathode.[168,170,171]

Zhang and coworkers[166] first used a composite composed of porphyrin COF and CNT (POF@CNT, Figure 17f) as the cathode in both liquid and flexible all-solid-state Zn-air batteries, which demonstrated superior performance. The liquid Zn-air battery exhibited a small voltage gap (0.71 V) and excellent stability (200 cycles, see Figure 17g), and the all-solid-state battery possessed a high energy efficiency (61.6% at 1.0 mA cm^{-2}). The prominent performance of the Zn-air battery was attributed to the synergistic effects of porphyrin COF (POF) and CNT. POF offered well-defined cobalt coordinated porphyrin active sites and hydrophilic surface, while interweaved CNT provided multiple electron pathways and promoted electron transport.

In 2019, Xiang and coworkers[172] proposed a novel strategy by in situ charge exfoliation in alkaline solutions to produce a highly stable COF solution. They realized high performance in Zn-air flow batteries by directly employing the solution as a

non-noble Pt catalyst. The COF had well-defined N-coordinate Fe single atom centers and conjugated backbones and proved as promising oxygen reduction catalysts. The COF solution even exhibited superior stability compared to commercial Pt/C-coated air electrodes. During the flowing process, no catalyst stripping or flooding occurred, and even no attenuation of discharge voltage in the same period was observed when the flow rate changed.

7. Other Advanced Batteries

The tunable structures of COFs also raise numerous attention in other advanced battery areas. For example, Ai et al.[95] coated COF on the surface of silicon nanoparticles as an artificial SSE layer in Li-Si battery and successfully reduced the silicon volume expansion. Li-Si batteries have been considered as one of the most promising electrochemical storage techniques due to their high theoretical capacity (4200 mAh g^{-1}, lithiated to $Li_{4.4}Si$) and abundant resources (second richest element).[144] However, serious volume expansion (≈360% for $Li_{4.4}Si$) caused accelerated electrode collapse and capacity fading, limiting their practical utilization and commercialization.[144] Additionally, a naturally formed SEI layer on silicon anode consumed lithium ions irreversibly and decreased the cycling performance of Li-Si batteries.[95,144] They found that silicon electrodes with COF coatings showed a reduced volume expansion (≈80%), while pure silicon electrodes suffered a serious volume expansion (≈160%). Thus, Si@COF exhibited an enhanced cycling performance with less capacity degradation compared to pristine silicon. Recently, Li-SeS_2 batteries also receive much attention as they combine the high specific capacity of sulfur and excellent conductivity of selenium. These batteries have a theoretical capacity as high as 1125 mAh g^{-1}.[102,173] However, Li-SeS_2 batteries suffer the same problems as Li-S batteries, where shuttle effects lead to loss of selenium/sulfur and thus cause poor cycling stability and low rate performance.[102,173] Wang et al.[102] employed a COF-coated separator and achieved superior rate performance and cycling stability in lithium-selenium sulfide batteries. The narrower cavity size of COF coatings effectively blocked the transport of polysulfide/polyselenide species in the electrolyte, and the methoxyl groups in the COF structure enhanced the Li^+ migration ability compared to the bare Celgard separator.

8. Conclusions and Perspectives

In this review, we summarized the recent applications of COFs in batteries, including LIBs, Li-S batteries, SIBs, PIBs, Li-CO_2 batteries, ZIBs, Zn-air batteries, and other advanced batteries. COFs are emerging crystalline porous materials with tailorable chemistry, tunable structure, and well-defined pores that show a promising future in batteries. However, the development of COF batteries is still at an infant stage, and many challenges remain to be tackled.

Most COFs are synthesized via solvothermal methods in a closed environment, so the large-scale synthesis of COFs for industrial applications is challenging due to the harsh reaction conditions. Though several room temperature synthesis strategies have been proposed,[174–178] the generality of these methods still needs further investigation in a large base. Therefore, the development of large-scale synthesis approaches without sacrificing the crystallinity and porosity of COFs is of paramount significance for their real applications.

Additionally, COFs are polycrystalline powders with many structural defects. It is challenging to control the degree of periodicity, crystal domain size, and porosity of many COFs. To date, COF single crystals were only reported by Ma et al.[179] through aniline modulation and Evans et al.[180] through seeded growth. Single crystal COFs could maximize the porosity of COFs and reduce the structure defects, which might enhance the electrochemical performance.

Low electron conductivity is one of the bottleneck problems for COFs in battery applications, which limits their good rate capability. Current strategies to improve their conductivity are constrained to in situ growth on the surface of CNT or graphene. The poor conductivity of COFs is primarily attributed to the weak interlayer interactions. Rational design of highly conjugated structures within the intralayer and strong interactions between the interlayers may serve as effective solutions. For example, hydrogen bonding between interlayers can increase interlayer interactions, and therefore the introduction of functional moieties (e.g., OH groups) that can form strong hydrogen bonding between different COF layers may serve as an effective solution. Designing electron-conductive organic linkers like thiophene and tetrathiafulvalene may enhance the intralayer electron conductivity of COFs. In addition, COFs have porous structures and can host electron conductive fillers inside the pores, and introducing conductive polymers (e.g., polypyrrole, poly(3,4-ethylenedioxythiophene) polystyrene sulfonate (PEDOT: PSS)) through in situ polymerization may significantly increase the conductivity of COFs. Furthermore, doping strategies including p-doping and n-doping have been widely used in polymers to improve the electron conductivity to metallic level. Doping of COFs using dopants like iodine may also serve as effective approaches to significantly improve their electron conductivity.

Bulk COFs with multiple stacking layers may bury a large number of active sites and lead to poor access and utilization of redox-active sites. Additionally, stacking layers increase the lithium diffusion pathways, cause sluggish Li-ion diffusion, and decrease the lithium transfer kinetics. To resolve these problems, delamination of bulk COFs into few-layer CONs proves to be an effective route to expose more redox-active sites and improve lithium transfer kinetics. However, large-scale exfoliation of bulk COFs into CONs is still challenging. It is also challenging to control the quality of CONs, including crystallinity, thickness, and planar size. Top-down strategies like chemical exfoliation or mechanical exfoliation are hard to maintain the thickness accurately and may bring more crystal defects and damage the large-size planar sheets. Bottom-up synthesis strategies are challenging to scale up and heavily depend on monomer chemistry though they are easier to produce highly crystalline and large-sized CONs.

The energy density of many organic electrodes, including COFs, is still lower than many inorganic electrodes. Rational design of COF structures and optimization of the density of redox-active sites on both backbones and substituents can be

effective solutions to improving the energy density of batteries. Exfoliation of bulk COFs into ultrathin nanosheets and alignment of pore channels can also help expose active sites to a maximum extent.

Though COFs demonstrate much higher stability than small organic molecules, the stability of COFs in organic electrolytes is still not enough and limits their long-term discharging-charging capability. Many COFs lose crystallinity after running for cycles and even degrade due to the dynamic linkage of COFs. Balancing the dynamic nature of COF linkages and electrochemical stability is essential. The development of highly crystalline and porous COFs with more stable linkages such as imide or amide might increase the stability of COFs in the electrolyte.

COFs for battery applications are still in the initial phase, and the metal ion storage mechanism is still controversial and ambiguous. Additionally, the ion and electron transport mechanisms are also unclear. Further insight into the ion storage mechanism and the electron/ion transport pathway through experimental investigations and theoretical simulations should be helpful.

To summarize, COFs provide new opportunities for building organic batteries and show many advantages over other organic materials such as tailorable compositions, crystalline structures, ordered cavities, and high surface areas. However, applications of COFs in battery fields are still in the early stage and face many challenges. Both experimental and theoretical efforts are expected to solve these challenges and improve the electrochemical performance of COFs.

Acknowledgements

D.Z. and G.X. contributed equally to this work. The authors acknowledge financial support from the Army Research Laboratory (W911NF-18-2-0062) and the Welch Foundation for Chemical Research (C-1888).

Conflict of Interest

The authors declare no conflict of interest.

Keywords

batteries, covalent organic frameworks, electrode materials, electrolytes, separators

Received: April 18, 2021
Published online: June 3, 2021

[1] L. Wang, Y. Han, X. Feng, J. Zhou, P. Qi, B. Wang, *Coord. Chem. Rev.* **2016**, *307*, 361.
[2] R. Zhao, Z. Liang, R. Zou, Q. Xu, *Joule* **2018**, *2*, 2235.
[3] W. Qi, J. G. Shapter, Q. Wu, T. Yin, G. Gao, D. Cui, *J. Mater. Chem. A* **2017**, *5*, 19521.
[4] Y. Lu, L. Yu, X. W. Lou (David), *Chem* **2018**, *4*, 972.
[5] S.-W. Kim, D.-H. Seo, X. Ma, G. Ceder, K. Kang, *Adv. Energy Mater.* **2012**, *2*, 710.
[6] X. Gao, Y. Dong, S. Li, J. Zhou, L. Wang, B. Wang, *Electrochem. Energy Rev.* **2020**, *3*, 81.
[7] X. Liu, C.-F. Liu, W.-Y. Lai, W. Huang, *Adv. Mater. Technol.* **2020**, *5*, 2000154.
[8] J. Li, X. Jing, Q. Li, S. Li, X. Gao, X. Feng, B. Wang, *Chem. Soc. Rev.* **2020**, *49*, 3565.
[9] T. Sun, J. Xie, W. Guo, D.-S. Li, Q. Zhang, *Adv. Energy Mater.* **2020**, *10*, 1904199.
[10] K. Zhang, K. O. Kirlikovali, R. S. Varma, Z. Jin, H. W. Jang, O. K. Farha, M. Shokouhimehr, *ACS Appl. Mater. Interfaces* **2020**, *12*, 27821.
[11] S. Kandambeth, K. Dey, R. Banerjee, *J. Am. Chem. Soc.* **2019**, *141*, 1807.
[12] R. K. Sharma, P. Yadav, M. Yadav, R. Gupta, P. Rana, A. Srivastava, R. Zbořil, R. S. Varma, M. Antonietti, M. B. Gawande, *Mater. Horiz.* **2020**, *7*, 411.
[13] D. Zhu, L. B. Alemany, W. Guo, R. Verduzco, *Polym. Chem.* **2020**, *11*, 4464.
[14] M. S. Lohse, T. Bein, *Adv. Funct. Mater.* **2018**, *28*, 1705553.
[15] M. Ding, X. Cai, H.-L. Jiang, *Chem. Sci.* **2019**, *10*, 10209.
[16] X. Yang, Y. Hu, N. Dunlap, X. Wang, S. Huang, Z. Su, S. Sharma, Y. Jin, F. Huang, X. Wang, S. Lee, W. Zhang, *Angew. Chem., Int. Ed.* **2020**, *59*, 20385.
[17] Q. Xu, S. Tao, Q. Jiang, D. Jiang, *J. Am. Chem. Soc.* **2018**, *140*, 7429.
[18] Q. Xu, S. Tao, Q. Jiang, D. Jiang, *Angew. Chem., Int. Ed.* **2020**, *59*, 4557.
[19] H. Liao, H. Ding, B. Li, X. Ai, C. Wang, *J. Mater. Chem. A* **2014**, *2*, 8854.
[20] H. Shin, D. Kim, H. J. Kim, J. Kim, K. Char, C. T. Yavuz, J. W. Choi, *Chem. Mater.* **2019**, *31*, 7910.
[21] F. Xu, S. Yang, G. Jiang, Q. Ye, B. Wei, H. Wang, *ACS Appl. Mater. Interfaces* **2017**, *9*, 37731.
[22] T. Kousksou, P. Bruel, A. Jamil, T. El Rhafiki, Y. Zeraouli, *Sol. Energy Mater. Sol. Cells* **2014**, *120*, 59.
[23] N. Nitta, F. Wu, J. T. Lee, G. Yushin, *Mater. Today* **2015**, *18*, 252.
[24] M. Li, J. Lu, Z. Chen, K. Amine, *Adv. Mater.* **2018**, *30*, 1800561.
[25] S. Goriparti, E. Miele, F. De Angelis, E. Di Fabrizio, R. Proietti Zaccaria, C. Capiglia, *J. Power Sources* **2014**, *257*, 421.
[26] Z. Chen, W. Zhang, Z. Yang, *Nanotechnology* **2019**, *31*, 012001.
[27] A. Manthiram, *Nat. Commun.* **2020**, *11*, 1550.
[28] M. Li, C. Wang, Z. Chen, K. Xu, J. Lu, *Chem. Rev.* **2020**, *120*, 6783.
[29] E. R. Logan, J. R. Dahn, *Trends Chem.* **2020**, *2*, 354.
[30] K. Xu, *Chem. Rev.* **2014**, *114*, 11503.
[31] W. Zhao, J. Yi, P. He, H. Zhou, *Electrochem. Energy Rev.* **2019**, *2*, 574.
[32] D. Zhou, D. Shanmukaraj, A. Tkacheva, M. Armand, G. Wang, *Chem* **2019**, *5*, 2326.
[33] P. Arora, Z. Zhang (John), *Chem. Rev.* **2004**, *104*, 4419.
[34] S. Bai, X. Liu, K. Zhu, S. Wu, H. Zhou, *Nat. Energy* **2016**, *1*, 16094.
[35] H. Lee, M. Yanilmaz, O. Toprakci, K. Fu, X. Zhang, *Energy Environ. Sci.* **2014**, *7*, 3857.
[36] J. Nunes-Pereira, C. M. Costa, S. Lanceros-Méndez, *J. Power Sources* **2015**, *281*, 378.
[37] G. Kucinskis, G. Bajars, J. Kleperis, *J. Power Sources* **2013**, *240*, 66.
[38] T. Kim, W. Song, D.-Y. Son, L. K. Ono, Y. Qi, *J. Mater. Chem. A* **2019**, *7*, 2942.
[39] M. E. Bhosale, S. Chae, J. M. Kim, J.-Y. Choi, *J. Mater. Chem. A* **2018**, *6*, 19885.
[40] Y. Liang, Y. Yao, *Joule* **2018**, *2*, 1690.
[41] Y. Lu, J. Chen, *Nat. Rev. Chem.* **2020**, *4*, 127.
[42] J.-Y. Hwang, S.-T. Myung, Y.-K. Sun, *Chem. Soc. Rev.* **2017**, *46*, 3529.
[43] L. Bai, Q. Gao, Y. Zhao, *J. Mater. Chem. A* **2016**, *4*, 14106.
[44] E. R. Wolfson, N. Xiao, L. Schkeryantz, W. Karl Haug, Y. Wu, P. L. McGrier, *Mol. Syst. Des. Eng.* **2020**, *5*, 97.
[45] S. Feng, H. Xu, C. Zhang, Y. Chen, J. Zeng, D. Jiang, J.-X. Jiang, *Chem. Commun.* **2017**, *53*, 11334.

[46] X. Yu, C. Li, Y. Ma, D. Li, H. Li, X. Guan, Y. Yan, V. Valtchev, S. Qiu, Q. Fang, *Microporous Mesoporous Mater.* **2020**, *299*, 110105.
[47] H. Yang, S. Zhang, L. Han, Z. Zhang, Z. Xue, J. Gao, Y. Li, C. Huang, Y. Yi, H. Liu, Y. Li, *ACS Appl. Mater. Interfaces* **2016**, *8*, 5366.
[48] H. Chen, Y. Zhang, C. Xu, M. Cao, H. Dou, X. Zhang, *Chem. - Eur. J.* **2019**, *25*, 15472.
[49] Z. Lei, Q. Yang, Y. Xu, S. Guo, W. Sun, H. Liu, L.-P. Lv, Y. Zhang, Y. Wang, *Nat. Commun.* **2018**, *9*, 576.
[50] S. Haldar, K. Roy, R. Kushwaha, S. Ogale, R. Vaidhyanathan, *Adv. Energy Mater.* **2019**, *9*, 1902428.
[51] H. Zhang, W. Sun, X. Chen, Y. Wang, *ACS Nano* **2019**, *13*, 14252.
[52] S. Haldar, K. Roy, S. Nandi, D. Chakraborty, D. Puthusseri, Y. Gawli, S. Ogale, R. Vaidhyanathan, *Adv. Energy Mater.* **2018**, *8*, 1702170.
[53] X. Chen, Y. Li, L. Wang, Y. Xu, A. Nie, Q. Li, F. Wu, W. Sun, X. Zhang, R. Vajtai, P. M. Ajayan, L. Chen, Y. Wang, *Adv. Mater.* **2019**, *31*, 1901640.
[54] B. Ball, C. Chakravarty, P. Sarkar, *J. Phys. Chem. C* **2019**, *123*, 30155.
[55] L. Fang, X. Cao, Z. Cao, *J. Phys.: Condens. Matter* **2019**, *31*, 205502.
[56] W. Zheng, C.-S. Tsang, L. Y. S. Lee, K.-Y. Wong, *Mater. Today Chem.* **2019**, *12*, 34.
[57] Z. Meng, R. M. Stolz, K. A. Mirica, *J. Am. Chem. Soc.* **2019**, *141*, 11929.
[58] X.-M. Lin, D.-Y. Wu, P. Gao, Z. Chen, M. Ruben, M. Fichtner, *Chem. Mater.* **2019**, *31*, 3239.
[59] H. V. Babu, M. G. M. Bai, M. Rajeswara Rao, *ACS Appl. Mater. Interfaces* **2019**, *11*, 11029.
[60] Z. Meng, R. M. Stolz, L. Mendecki, K. A. Mirica, *Chem. Rev.* **2019**, *119*, 478.
[61] H. Kang, H. Liu, C. Li, L. Sun, C. Zhang, H. Gao, J. Yin, B. Yang, Y. You, K.-C. Jiang, H. Long, S. Xin, *ACS Appl. Mater. Interfaces* **2018**, *10*, 37023.
[62] W. A. Braunecker, K. E. Hurst, K. G. Ray, Z. R. Owczarczyk, M. B. Martinez, N. Leick, A. Keuhlen, A. Sellinger, J. C. Johnson, *Cryst. Growth Des.* **2018**, *18*, 4160.
[63] P. Bhanja, S. Mishra, K. Manna, A. Mallick, K. Das Saha, A. Bhaumik, *ACS Appl. Mater. Interfaces* **2017**, *9*, 31411.
[64] K. Sakaushi, E. Hosono, G. Nickerl, H. Zhou, S. Kaskel, J. Eckert, *J. Power Sources* **2014**, *245*, 553.
[65] X. Chen, H. Zhang, C. Ci, W. Sun, Y. Wang, *ACS Nano* **2019**, *13*, 3600.
[66] F. Xu, S. Jin, H. Zhong, D. Wu, X. Yang, X. Chen, H. Wei, R. Fu, D. Jiang, *Sci. Rep.* **2015**, *5*, 8225.
[67] Z. Luo, L. Liu, J. Ning, K. Lei, Y. Lu, F. Li, J. Chen, *Angew. Chem., Int. Ed.* **2018**, *57*, 9443.
[68] Z. Wang, Y. Li, P. Liu, Q. Qi, F. Zhang, G. Lu, X. Zhao, X. Huang, *Nanoscale* **2019**, *11*, 5330.
[69] G. Wang, N. Chandrasekhar, B. P. Biswal, D. Becker, S. Paasch, E. Brunner, M. Addicoat, M. Yu, R. Berger, X. Feng, *Adv. Mater.* **2019**, *31*, 1901478.
[70] M. R. Al Hassan, A. Sen, T. Zaman, M. S. Mostari, *Mater. Today Chem.* **2019**, *11*, 225.
[71] C.-J. Yao, Z. Wu, J. Xie, F. Yu, W. Guo, Z. J. Xu, D.-S. Li, S. Zhang, Q. Zhang, *ChemSusChem* **2019**, *13*, 2457.
[72] D.-H. Yang, Z.-Q. Yao, D. Wu, Y.-H. Zhang, Z. Zhou, X.-H. Bu, *J. Mater. Chem. A* **2016**, *4*, 18621.
[73] J. Xie, P. Gu, Q. Zhang, *ACS Energy Lett.* **2017**, *2*, 1985.
[74] S. Muench, A. Wild, C. Friebe, B. Häupler, T. Janoschka, U. S. Schubert, *Chem. Rev.* **2016**, *116*, 9438.
[75] Q. Fang, Z. Zhuang, S. Gu, R. B. Kaspar, J. Zheng, J. Wang, S. Qiu, Y. Yan, *Nat. Commun.* **2014**, *5*, 4503.
[76] Q. Fang, J. Wang, S. Gu, R. B. Kaspar, Z. Zhuang, J. Zheng, H. Guo, S. Qiu, Y. Yan, *J. Am. Chem. Soc.* **2015**, *137*, 8352.
[77] J. Maschita, T. Banerjee, G. Savasci, F. Haase, C. Ochsenfeld, B. V. Lotsch, *Angew. Chem., Int. Ed.* **2020**, *59*, 15750.
[78] X. Guan, H. Li, Y. Ma, M. Xue, Q. Fang, Y. Yan, V. Valtchev, S. Qiu, *Nat. Chem.* **2019**, *11*, 587.
[79] H.-L. Qian, F.-L. Meng, C.-X. Yang, X.-P. Yan, *Angew. Chem., Int. Ed.* **2020**, *59*, 17607.
[80] P. J. Waller, Y. S. AlFaraj, C. S. Diercks, N. N. Jarenwattananon, O. M. Yaghi, *J. Am. Chem. Soc.* **2018**, *140*, 9099.
[81] K. Wang, Z. Jia, Y. Bai, X. Wang, S. E. Hodgkiss, L. Chen, S. Y. Chong, X. Wang, H. Yang, Y. Xu, F. Feng, J. W. Ward, A. I. Cooper, *J. Am. Chem. Soc.* **2020**, *142*, 11131.
[82] X. Li, K. P. Loh, *ACS Mater. Lett.* **2019**, *1*, 327.
[83] L. Zhang, K. Yang, J. Mi, L. Lu, L. Zhao, L. Wang, Y. Li, H. Zeng, *Adv. Energy Mater.* **2015**, *5*, 1501294.
[84] G. Zhang, Y. Hong, Y. Nishiyama, S. Bai, S. Kitagawa, S. Horike, *J. Am. Chem. Soc.* **2019**, *141*, 1227.
[85] Y. Du, H. Yang, J. M. Whiteley, S. Wan, Y. Jin, S.-H. Lee, W. Zhang, *Angew. Chem., Int. Ed.* **2016**, *55*, 1737.
[86] Y. Zhang, J. Duan, D. Ma, P. Li, S. Li, H. Li, J. Zhou, X. Ma, X. Feng, B. Wang, *Angew. Chem., Int. Ed.* **2017**, *56*, 16313.
[87] H. Chen, H. Tu, C. Hu, Y. Liu, D. Dong, Y. Sun, Y. Dai, S. Wang, H. Qian, Z. Lin, L. Chen, *J. Am. Chem. Soc.* **2018**, *140*, 896.
[88] Z. Guo, Y. Zhang, Y. Dong, J. Li, S. Li, P. Shao, X. Feng, B. Wang, *J. Am. Chem. Soc.* **2019**, *141*, 1923.
[89] Y. Hu, N. Dunlap, S. Wan, S. Lu, S. Huang, I. Sellinger, M. Ortiz, Y. Jin, S. Lee, W. Zhang, *J. Am. Chem. Soc.* **2019**, *141*, 7518.
[90] K. Jeong, S. Park, G. Y. Jung, S. H. Kim, Y.-H. Lee, S. K. Kwak, S.-Y. Lee, *J. Am. Chem. Soc.* **2019**, *141*, 5880.
[91] D. A. Vazquez-Molina, G. S. Mohammad-Pour, C. Lee, M. W. Logan, X. Duan, J. K. Harper, F. J. Uribe-Romo, *J. Am. Chem. Soc.* **2016**, *138*, 9767.
[92] D. Chen, S. Huang, L. Zhong, S. Wang, M. Xiao, D. Han, Y. Meng, *Adv. Funct. Mater.* **2020**, *30*, 1907717.
[93] Z. Zhao, W. Chen, S. Impeng, M. Li, R. Wang, Y. Liu, L. Zhang, L. Dong, J. Unruangsri, C. Peng, C. Wang, S. Namuangruk, S.-Y. Lee, Y. Wang, H. Lu, J. Guo, *J. Mater. Chem. A* **2020**, *8*, 3459.
[94] T. Zhou, Y. Zhao, J. W. Choi, A. Coskun, *Angew. Chem., Int. Ed.* **2019**, *58*, 16795.
[95] Q. Ai, Q. Fang, J. Liang, X. Xu, T. Zhai, G. Gao, H. Guo, G. Han, L. Ci, J. Lou, *Nano Energy* **2020**, *72*, 104657.
[96] D. Dong, H. Zhang, B. Zhou, Y. Sun, H. Zhang, M. Cao, J. Li, H. Zhou, H. Qian, Z. Lin, H. Chen, *Chem. Commun.* **2019**, *55*, 1458.
[97] V. Deimede, C. Elmasides, *Energy Technol.* **2015**, *3*, 453.
[98] Y. Wen, X. Wang, Y. Yang, M. Liu, W. Tu, M. Xu, G. Sun, S. Kawaguchi, G. Cao, W. Li, *J. Mater. Chem. A* **2019**, *7*, 26540.
[99] Q. X. Shi, H. J. Pei, N. You, J. Wu, X. Xiang, Q. Xia, X. L. Xie, S. B. Jin, Y. S. Ye, *Chem. Eng. J.* **2019**, *375*, 121977.
[100] J. Wang, L. Si, Q. Wei, X. Hong, S. Cai, Y. Cai, *ACS Appl. Nano Mater.* **2018**, *1*, 132.
[101] Q. Xu, K. Zhang, J. Qian, Y. Guo, X. Song, H. Pan, D. Wang, X. Li, *ACS Appl. Energy Mater.* **2019**, *2*, 5793.
[102] Y. Yang, X.-J. Hong, C.-L. Song, G.-H. Li, Y.-X. Zheng, D.-D. Zhou, M. Zhang, Y.-P. Cai, H. Wang, *J. Mater. Chem. A* **2019**, *7*, 16323.
[103] W. Xue, Z. Shi, L. Suo, C. Wang, Z. Wang, H. Wang, K. P. So, A. Maurano, D. Yu, Y. Chen, L. Qie, Z. Zhu, G. Xu, J. Kong, J. Li, *Nat. Energy* **2019**, *4*, 374.
[104] G. Xu, A. Kushima, J. Yuan, H. Dou, W. Xue, X. Zhang, X. Yan, J. Li, *Energy Environ. Sci.* **2017**, *10*, 2544.
[105] J. He, A. Manthiram, *Energy Storage Mater.* **2019**, *20*, 55.
[106] A. Manthiram, Y. Fu, S.-H. Chung, C. Zu, Y.-S. Su, *Chem. Rev.* **2014**, *114*, 11751.
[107] X. Zhao, G. Cheruvally, C. Kim, K.-K. Cho, H.-J. Ahn, K.-W. Kim, J.-H. Ahn, *J. Electrochem. Sci. Technol.* **2016**, *7*, 97.
[108] H.-J. Peng, J.-Q. Huang, X.-B. Cheng, Q. Zhang, *Adv. Energy Mater.* **2017**, *7*, 1700260.
[109] G. Xu, B. Ding, J. Pan, P. Nie, L. Shen, X. Zhang, *J. Mater. Chem. A* **2014**, *2*, 12662.

[110] G. Xu, B. Ding, P. Nie, L. Shen, J. Wang, X. Zhang, *Chem. - Eur. J.* **2013**, *19*, 12306.
[111] C. Tang, Q. Zhang, M.-Q. Zhao, J.-Q. Huang, X.-B. Cheng, G.-L. Tian, H.-J. Peng, F. Wei, *Adv. Mater.* **2014**, *26*, 6100.
[112] L. Ji, M. Rao, H. Zheng, L. Zhang, Y. Li, W. Duan, J. Guo, E. J. Cairns, Y. Zhang, *J. Am. Chem. Soc.* **2011**, *133*, 18522.
[113] J. Zheng, J. Tian, D. Wu, M. Gu, W. Xu, C. Wang, F. Gao, M. H. Engelhard, J.-G. Zhang, J. Liu, J. Xiao, *Nano Lett.* **2014**, *14*, 2345.
[114] G. Xu, B. Ding, P. Nie, L. Shen, H. Dou, X. Zhang, *ACS Appl. Mater. Interfaces* **2014**, *6*, 194.
[115] L. Xiao, Y. Cao, J. Xiao, B. Schwenzer, M. H. Engelhard, L. V. Saraf, Z. Nie, G. J. Exarhos, J. Liu, *Adv. Mater.* **2012**, *24*, 1176.
[116] G. Xu, Q. Yan, A. Kushima, X. Zhang, J. Pan, J. Li, *Nano Energy* **2017**, *31*, 568.
[117] A. G. Simmonds, J. J. Griebel, J. Park, K. R. Kim, W. J. Chung, V. P. Oleshko, J. Kim, E. T. Kim, R. S. Glass, C. L. Soles, Y.-E. Sung, K. Char, J. Pyun, *ACS Macro Lett.* **2014**, *3*, 229.
[118] S. Yuan, J. L. Bao, L. Wang, Y. Xia, D. G. Truhlar, Y. Wang, *Adv. Energy Mater.* **2016**, *6*, 1501733.
[119] Y. Qiu, W. Li, W. Zhao, G. Li, Y. Hou, M. Liu, L. Zhou, F. Ye, H. Li, Z. Wei, S. Yang, W. Duan, Y. Ye, J. Guo, Y. Zhang, *Nano Lett.* **2014**, *14*, 4821.
[120] X. Zhang, K. Chen, Z. Sun, G. Hu, R. Xiao, H.-M. Cheng, F. Li, *Energy Environ. Sci.* **2020**, *13*, 1076.
[121] F. Xu, S. Yang, X. Chen, Q. Liu, H. Li, H. Wang, B. Wei, D. Jiang, *Chem. Sci.* **2019**, *10*, 6001.
[122] Y. Meng, G. Lin, H. Ding, H. Liao, C. Wang, *J. Mater. Chem. A* **2018**, *6*, 17186.
[123] S. H. Je, H. J. Kim, J. Kim, J. W. Choi, A. Coskun, *Adv. Funct. Mater.* **2017**, *27*, 1703947.
[124] D.-G. Wang, N. Li, Y. Hu, S. Wan, M. Song, G. Yu, Y. Jin, W. Wei, K. Han, G.-C. Kuang, W. Zhang, *ACS Appl. Mater. Interfaces* **2018**, *10*, 42233.
[125] B.-Q. Li, S.-Y. Zhang, L. Kong, H.-J. Peng, Q. Zhang, *Adv. Mater.* **2018**, *30*, 1707483.
[126] Z. A. Ghazi, L. Zhu, H. Wang, A. Naeem, A. M. Khattak, B. Liang, N. A. Khan, Z. Wei, L. Li, Z. Tang, *Adv. Energy Mater.* **2016**, *6*, 1601250.
[127] H. Liao, H. Wang, H. Ding, X. Meng, H. Xu, B. Wang, X. Ai, C. Wang, *J. Mater. Chem. A* **2016**, *4*, 7416.
[128] X. Yang, B. Dong, H. Zhang, R. Ge, Y. Gao, H. Zhang, *RSC Adv.* **2015**, *5*, 86137.
[129] X. Zhang, Z. Wang, L. Yao, Y. Mai, J. Liu, X. Hua, H. Wei, *Mater. Lett.* **2018**, *213*, 143.
[130] X. Zhang, L. Yao, S. Liu, Q. Zhang, Y. Mai, N. Hu, H. Wei, *Mater. Today Energy* **2018**, *7*, 141.
[131] G. Xu, Q. Yan, P. Bai, H. Dou, P. Nie, X. Zhang, *ChemistrySelect* **2019**, *4*, 698.
[132] G. Xu, Q. Yan, S. Wang, A. Kushima, P. Bai, K. Liu, X. Zhang, Z. Tang, J. Li, *Chem. Sci.* **2017**, *8*, 6619.
[133] G. Xu, D. Yu, D. Zheng, S. Wang, W. Xue, X. E. Cao, H. Zeng, X. Xiao, M. Ge, W.-K. Lee, M. Zhu, *iScience* **2020**, *23*, 101576.
[134] J. Yoo, S.-J. Cho, G. Y. Jung, S. H. Kim, K.-H. Choi, J.-H. Kim, C. K. Lee, S. K. Kwak, S.-Y. Lee, *Nano Lett.* **2016**, *16*, 3292.
[135] Y. Cao, C. Liu, M. Wang, H. Yang, S. Liu, H. Wang, Z. Yang, F. Pan, Z. Jiang, J. Sun, *Energy Storage Mater.* **2020**, *29*, 207.
[136] S. N. Talapaneni, T. H. Hwang, S. H. Je, O. Buyukcakir, J. W. Choi, A. Coskun, *Angew. Chem., Int. Ed.* **2016**, *55*, 3106.
[137] Z. Xiao, L. Li, Y. Tang, Z. Cheng, H. Pan, D. Tian, R. Wang, *Energy Storage Mater.* **2018**, *12*, 252.
[138] X. Chen, Y. Xu, F.-H. Du, Y. Wang, *Small Methods* **2019**, *3*, 1900338.
[139] J. Wang, L. Si, Q. Wei, X. Hong, L. Lin, X. Li, J. Chen, P. Wen, Y. Cai, *J. Energy Chem.* **2019**, *28*, 54.
[140] J. Wang, W. Qin, X. Zhu, Y. Teng, *Energy* **2020**, *199*, 117372.
[141] J. Kim, A. Elabd, S.-Y. Chung, A. Coskun, J. W. Choi, *Chem. Mater.* **2020**, *32*, 4185.
[142] R. Gomes, A. J. Bhattacharyya, *ACS Sustainable Chem. Eng.* **2020**, *8*, 5946.
[143] J.-Y. Hwang, S.-T. Myung, Y.-K. Sun, *Adv. Funct. Mater.* **2018**, *28*, 1802938.
[144] X. Zuo, J. Zhu, P. Müller-Buschbaum, Y.-J. Cheng, *Nano Energy* **2017**, *31*, 113.
[145] K. Chayambuka, G. Mulder, D. L. Danilov, P. H. L. Notten, *Adv. Energy Mater.* **2018**, *8*, 1800079.
[146] Y. Liang, W.-H. Lai, Z. Miao, S.-L. Chou, *Small* **2018**, *14*, 1702514.
[147] J. C. Pramudita, D. Sehrawat, D. Goonetilleke, N. Sharma, *Adv. Energy Mater.* **2017**, *7*, 1602911.
[148] R. Rajagopalan, Y. Tang, X. Ji, C. Jia, H. Wang, *Adv. Funct. Mater.* **2020**, *30*, 1909486.
[149] D. Su, A. McDonagh, S.-Z. Qiao, G. Wang, *Adv. Mater.* **2017**, *29*, 1604007.
[150] B. Chandra Patra, S. Kanti Das, A. Ghosh, A. R. K, P. Moitra, M. Addicoat, S. Mitra, A. Bhaumik, S. Bhattacharya, A. Pradhan, *J. Mater. Chem. A* **2018**, *6*, 16655.
[151] Z. Zhang, M. Li, Y. Gao, Z. Wei, M. Zhang, C. Wang, Y. Zeng, B. Zou, G. Chen, F. Du, *Adv. Funct. Mater.* **2018**, *28*, 1802684.
[152] S.-Y. Li, W.-H. Li, X.-L. Wu, Y. Tian, J. Yue, G. Zhu, *Chem. Sci.* **2019**, *10*, 7695.
[153] M.-S. Kim, W.-J. Lee, S.-M. Paek, J. K. Park, *ACS Appl. Mater. Interfaces* **2018**, *10*, 32102.
[154] S. Haldar, D. Kaleeswaran, D. Rase, K. Roy, S. Ogale, V. Ramanathan, *Nanoscale Horiz.* **2020**, *5*, 1264.
[155] R. Shi, L. Liu, Y. Lu, C. Wang, Y. Li, L. Li, Z. Yan, J. Chen, *Nat. Commun.* **2020**, *11*, 178.
[156] S. Gu, S. Wu, L. Cao, M. Li, N. Qin, J. Zhu, Z. Wang, Y. Li, Z. Li, J. Chen, Z. Lu, *J. Am. Chem. Soc.* **2019**, *141*, 9623.
[157] X. Mu, H. Pan, P. He, H. Zhou, *Adv. Mater.* **2019**, *32*, 1903790.
[158] J. Xie, Y. Wang, *Acc. Chem. Res.* **2019**, *52*, 1721.
[159] S. Huang, D. Chen, C. Meng, S. Wang, S. Ren, D. Han, M. Xiao, L. Sun, Y. Meng, *Small* **2019**, *15*, 1904830.
[160] X. Li, H. Wang, Z. Chen, H.-S. Xu, W. Yu, C. Liu, X. Wang, K. Zhang, K. Xie, K. P. Loh, *Adv. Mater.* **2019**, *31*, 1905879.
[161] W. Xu, Y. Wang, *Nano-Micro Lett.* **2019**, *11*, 90.
[162] G. Fang, J. Zhou, A. Pan, S. Liang, *ACS Energy Lett.* **2018**, *3*, 2480.
[163] J. Shin, J. Lee, Y. Park, J. W. Choi, *Chem. Sci.* **2020**, *11*, 2028.
[164] A. K. M, M. Ghosh, V. Vijayakumar, A. Halder, M. Nurhuda, S. Kumar, M. Addicoat, S. Kurungot, R. Banerjee, *Chem. Sci.* **2019**, *10*, 8889.
[165] W. Wang, V. S. Kale, Z. Cao, S. Kandambeth, W. Zhang, J. Ming, P. T. Parvatkar, E. Abou-Hamad, O. Shekhah, L. Cavallo, M. Eddaoudi, H. N. Alshareef, *ACS Energy Lett.* **2020**, *5*, 2256.
[166] B.-Q. Li, S.-Y. Zhang, B. Wang, Z.-J. Xia, C. Tang, Q. Zhang, *Energy Environ. Sci.* **2018**, *11*, 1723.
[167] J. Fu, R. Liang, G. Liu, A. Yu, Z. Bai, L. Yang, Z. Chen, *Adv. Mater.* **2019**, *31*, 1805230.
[168] Y. Li, H. Dai, *Chem. Soc. Rev.* **2014**, *43*, 5257.
[169] J. Zhang, Q. Zhou, Y. Tang, L. Zhang, Y. Li, *Chem. Sci.* **2019**, *10*, 8924.
[170] J. Fu, Z. P. Cano, M. G. Park, A. Yu, M. Fowler, Z. Chen, *Adv. Mater.* **2017**, *29*, 1604685.
[171] Y. Li, J. Lu, *ACS Energy Lett.* **2017**, *2*, 1370.
[172] P. Peng, L. Shi, F. Huo, S. Zhang, C. Mi, Y. Cheng, Z. Xiang, *ACS Nano* **2019**, *13*, 878.
[173] W. Kim, J. Lee, S. Lee, K. Eom, C. Pak, H.-J. Kim, *Appl. Surf. Sci.* **2020**, *512*, 145632.
[174] M. Matsumoto, R. R. Dasari, W. Ji, C. H. Feriante, T. C. Parker, S. R. Marder, W. R. Dichtel, *J. Am. Chem. Soc.* **2017**, *139*, 4999.

[175] M. Zhang, J. Chen, S. Zhang, X. Zhou, L. He, M. V. Sheridan, M. Yuan, M. Zhang, L. Chen, X. Dai, F. Ma, J. Wang, J. Hu, G. Wu, X. Kong, R. Zhou, T. E. Albrecht-Schmitt, Z. Chai, S. Wang, *J. Am. Chem. Soc.* **2020**, *142*, 9169.
[176] S. Karak, S. Kandambeth, B. P. Biswal, H. S. Sasmal, S. Kumar, P. Pachfule, R. Banerjee, *J. Am. Chem. Soc.* **2017**, *139*, 1856.
[177] B. P. Biswal, S. Chandra, S. Kandambeth, B. Lukose, T. Heine, R. Banerjee, *J. Am. Chem. Soc.* **2013**, *135*, 5328.
[178] D. Zhu, Z. Zhang, L. B. Alemany, Y. Li, N. Nnorom, M. Barnes, S. Khalil, M. M. Rahman, P. M. Ajayan, R. Verduzco, *Chem. Mater.* **2021**, *33*, 3394.
[179] T. Ma, E. A. Kapustin, S. X. Yin, L. Liang, Z. Zhou, J. Niu, L.-H. Li, Y. Wang, J. Su, J. Li, X. Wang, W. D. Wang, W. Wang, J. Sun, O. M. Yaghi, *Science* **2018**, *361*, 48.
[180] A. M. Evans, L. R. Parent, N. C. Flanders, R. P. Bisbey, E. Vitaku, M. S. Kirschner, R. D. Schaller, L. X. Chen, N. C. Gianneschi, W. R. Dichtel, *Science* **2018**, *361*, 52.

Dongyang Zhu received his Ph.D. degrees (May 2021) in Chemical and Biomolecular Engineering at Rice University, USA. His current research focuses on design and synthesis of covalent organic frameworks, and investigations on their fundamental properties, electrochemical energy storage, photocatalysis and environmental applications.

Guiyin Xu received his Ph.D. degree from Nanjing University of Aeronautics and Astronautics (NUAA) under the co-supervision of Prof. Xiaogang Zhang (NUAA) and Prof. Ju Li (MIT). Now, he is a Postdoctoral Associate in Ju Li's group at MIT. His research focuses on advanced electrode materials for green energy, and functional materials for environmental remediation.

Muhammad M. Rahman is a research scientist in the Department of Materials Science and NanoEngineering at Rice University. He received his Ph.D. from Cornell University and B.Sc. from Bangladesh University of Engineering and Technology (BUET). His research interests focus on the development of high-performance materials using multifunctional fibers, polymers, and nanomaterials for load-bearing structures, textiles, energy, and environmental applications.

Rafael Verduzco is a Professor of Chemical and Biomolecular Engineering and Materials Sciences and NanoEngineering at Rice University. Verduzco received his Ph.D. in Chemical Engineering from the California Institute of Technology in 2007 and his BS in Chemical Engineering from Rice University in 2001. The Verduzco laboratory uses a combination of materials chemistry and multiscale characterization tools to design new materials and address fundamental challenges in polymeric and organic materials. A major area of emphasis is on the design and development of covalent organic frameworks for applications in energy storage and remediation.

Pulickel M. Ajayan is the Benjamin M. and Mary Greenwood Anderson Professor in Engineering at Rice University. He is the founding chair of Rice University's Materials Science and NanoEngineering department and holds joint appointments with the Department of Chemistry and Department of Chemical and Biomolecular Engineering. His research interests include synthesis and structure–property relations of nanostructures and nanocomposites, materials science, and applications of nanomaterials, energy storage, and phase stability in nanoscale systems.